ELSEVIER

Journal of Structural Geology 28 (2006) 850–867

JOURNAL OF STRUCTURAL GEOLOGY

www.elsevier.com/locate/jsg

The role of fractures in the structural interpretation of Sheep Mountain Anticline, Wyoming

Nicolas Bellahsen *,[1], Patricia Fiore, David D. Pollard

Department of Geological & Environmental Sciences, Stanford University, Stanford, CA 94305-2115, USA

Received 3 May 2005; received in revised form 5 January 2006; accepted 28 January 2006
Available online 3 April 2006

Abstract

The development of fractures in the sedimentary layers of Sheep Mountain Anticline, a Laramide asymmetric fault-cored fold of the Bighorn Basin, is documented and interpreted to constrain the kinematic evolution of the fold. The fracture pattern is interpreted to identify five main fracture sets. A fracture set striking 110° (Set I), oblique to the future fold trend, is interpreted as a regional fracture set that predates Laramide compression. A joint set (Set II), striking 045° and present in the hinge and backlimb, is related to the NE-oriented Laramide compression just prior to and during initial anticline growth. Joints striking 135° (Set III), parallel to the fold trend, are found within the hinge and are interpreted to have developed in response to the bending of layers. The two youngest fracture sets are attributed to a late stage of fold growth: a joint set (Set IV) in the backlimb striking parallel to the Set I fractures, but vertical; and a fracture set in the forelimb consisting of Set I fractures reactivated as reverse faults. The relative chronology, mode of formation (opening vs. shearing), and structural locations of these fractures suggest the following kinematics of folding at Sheep Mountain Anticline: little or no lateral fold propagation; no hinge migration; and limb rotation with only minor limb flexure and stretching.

Keywords: Fracture; Fold; Joints; Thrust fault; Sheep Mountain; Bighorn Basin

1. Introduction

Fold–fracture relationships were conceptualized in the late 1960s and 1970s (Price, 1966; Stearns, 1968; Friedman, 1969; Stearns and Friedman, 1972; Price and Cosgrove, 1990). These conceptual models have three shortcomings, which have been addressed in recent investigations. First, they do not consider the temporal evolution of the fold. The fractures described in these models are correlated with final fold geometry, without consideration of either the effect of the initial and transitional fold shapes on fracture development, or fracture evolution during fold growth (Fischer and Wilkerson, 2000). Second, they neglect to account for the influence of pre-existing fractures (Guiton et al., 2003a,b; Bergbauer and Pollard, 2004). Third, they disregard the effect of primary faults, which are often associated with fold formation (Johnson and Johnson, 2002; Savage and Cooke, 2004). Fault slip perturbs the surrounding stress field (Hafner, 1951; Lajtai, 1969; Couples, 1977; Segall and Pollard, 1980; Pollard and Segall, 1987; Rawnsley et al., 1992; Reches and Lockner, 1994; Homberg et al., 1997; Martel and Boger, 1998; Kattenhorn et al., 2000; Bourne and Willemse, 2001; Maerten et al., 2002) on the scale of fault length and can affect fracture formation within this zone of influence. In this paper we document the distribution and characteristics of fractures at Sheep Mountain Anticline, we develop fold–fracture relationships that account for these observations, and we use these data to interpret fold evolution.

Kinematic models attempt to unravel fold evolution with time through both backward and forward modeling, with the present-day shape of the fold as calibration (e.g. Suppe, 1985; Jamison, 1987; Mitra, 1990; Erslev, 1991; Cristallini and Allmendinger, 2002; Bump, 2003). These models are based on kinematic assumptions such as hinge migration (Suppe, 1983; Beutner and Diegel, 1985; Allmendinger, 1998) or fixed hinge (Erslev, 1991; McConnell, 1994; Spang and McConnell, 1997), rotating limbs (Erslev, 1991) or fixed limb dip (Suppe, 1983; Suppe and Medwedeff, 1990). Recent studies have suggested that a fold may attain its maximum (along-strike) length very early during its evolution (e.g. Armstrong and Bartley, 1993; Cristallini and Allmendinger, 2001; Bernal and Hardy, 2002; Fischer and Christensen, 2004). In contrast,

* Corresponding author. Tel.: +33 1 44 27 52 56.
E-mail address: nicolasb@pangea.stanford.edu (N. Bellahsen).
[1] Now at Laboratoire de Tectonique, Université Pierre et Marie Curie, Paris, France

0191-8141/$ - see front matter © 2006 Elsevier Ltd. All rights reserved.
doi:10.1016/j.jsg.2006.01.013

other workers have inferred that fold tips propagate laterally through time (e.g. Fischer and Wilkerson, 2000), maintaining that vertical displacement on a fault is accompanied by increasing length (Cowie and Scholz, 1992; Dawers et al., 1993; Peacock and Sanderson, 1991). We propose that the kinematics of a thrust fault-related fold can be constrained through an examination of the deformation recorded by joints, faults, and deformation bands within the folded layers (Nickelsen, 1979; Dunne, 1986; Engelder et al., 1997; Fischer and Christensen, 2004). The chronology of these mesoscopic structures, when combined with their geometries and deformation modes, provides insight into the structural setting at the time of their formation. We show how inferences are made that associate each fracture set with a particular stage of fold evolution (pre-, early-, syn-, late-, or post-folding). The timing and locations of these fractures thereby inform an improved kinematic model of folding at the Sheep Mountain Anticline.

Recent studies have attempted to constrain the unknown parameters of folding at various field sites, making use of mechanical models, for which the present-day fold shape and fracture distributions serve as calibration (e.g. Shamir and Eyal, 1995; Nino et al., 1998; Zhang et al., 2000; Johnson and Johnson, 2002; Savage and Cooke, 2004, and references therein). For example, Nino et al. (1998) examined the role of fault dip, layer thickness, and bedding-parallel slip with elasto-plastic models that replicate the shape of the Jabal Mquebra anticline in Syria. Johnson and Johnson (2002) showed that viscous models reproduce the shape of some of the Rocky Mountain foreland basement-involved folds when the appropriate underlying fault geometry, magnitude of cover anisotropy, and nature of the basement–cover contact are prescribed. Savage and Cooke (2004) showed how the geometry of a subsidiary fault at Sheep Mountain Anticline, Wyoming can be developed using elastic models. Mechanical models also provide the opportunity to investigate fold–fracture relationships based on stress field evolution (Guiton et al., 2003a,b).

We focus our study on Sheep Mountain Anticline, Wyoming (Fig. 1), which is widely known for its exceptional outcrops. The most notable exposures are located in the

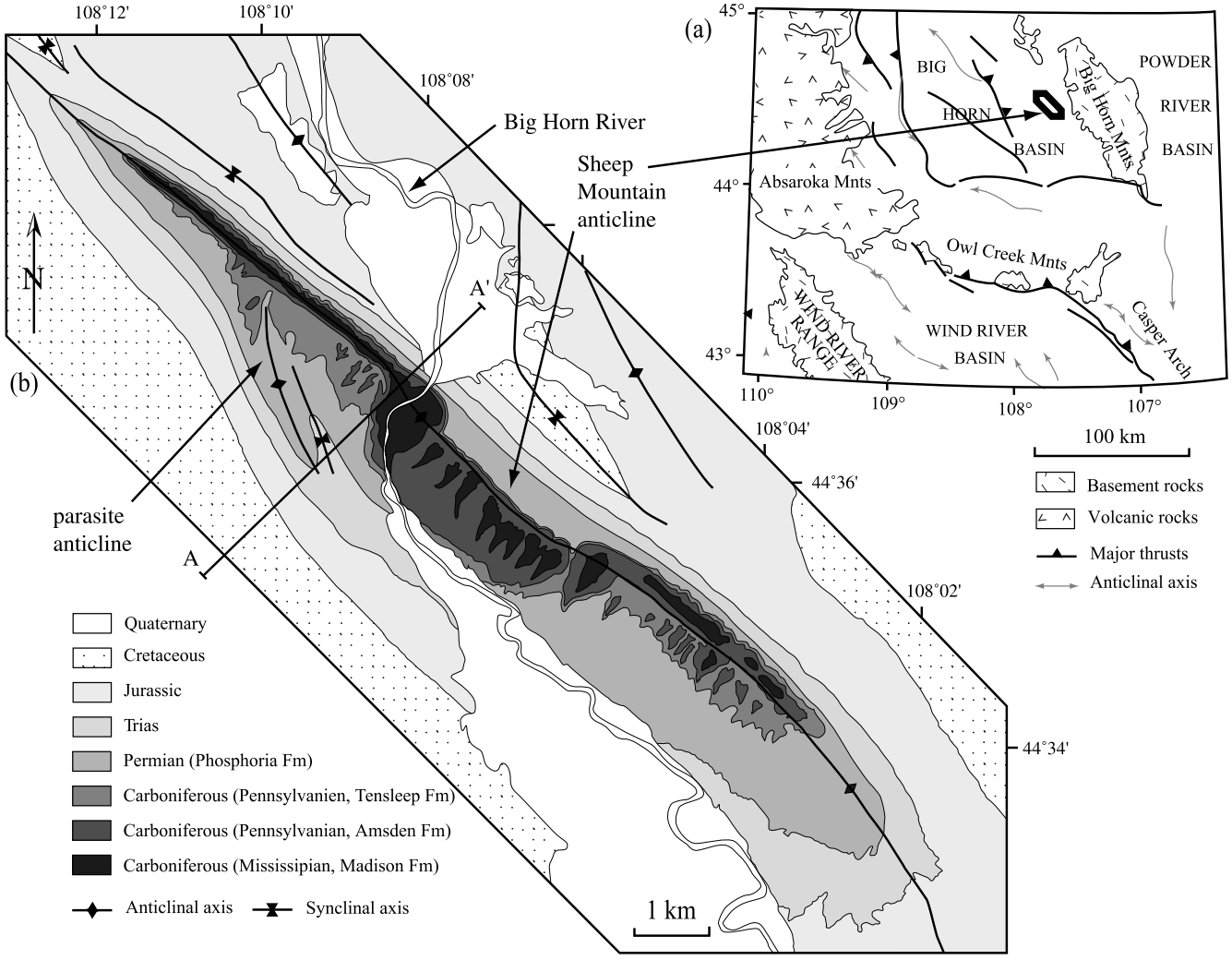

Fig. 1. Geologic and tectonic maps of Sheep Mountain anticline. (a) Detail of the Wyoming tectonic map with a polygon outlining the location of the anticline. (b) Geological map of the anticline from Rioux (1994). The line A–A′ is the location of the cross-section shown in Fig. 2.

Bighorn River canyon cut, which runs approximately perpendicular to the axial trend of the anticline. Studies over the past two decades have contributed to an understanding of the large-scale deformation at Sheep Mountain (Hennier and Spang, 1983; Stone, 1993; Forster et al., 1996; Savage and Cooke, 2004), particularly the underlying fault geometry. Recently, a new geometric and kinematic model was developed for the subsurface structure of the anticline (Stanton and Erslev, 2004). From the interpretation of three 2D seismic reflection lines, as well as surface maps from previous studies (Rioux, 1958, 1994; Hennier, 1984) and stratigraphic picks within exploration wells, Stanton and Erslev (2004) interpreted the fold to have resulted from slip along a SW-dipping basement fault that was followed by slip on a NE-dipping fault (Fig. 2).

Although the underlying fault geometry at Sheep Mountain has received attention, knowledge of the fracture patterns is limited. Harris et al. (1960) described several fracture sets in the Sheep Mountain area as a function of bed thickness and lithology. They interpreted the systematic (planar, parallel, repetitious) fracture sets as 'of compressional deformational origin' and 'related to shear stresses'. However, diagnostic evidence for such an interpretation (e.g. see Pollard and Aydin, 1988) was not reported; these interpretations apparently were based purely on the geometry of the fracture sets. Furthermore, the fracture orientations were not reported, effects of bedding orientation on fracture geometry were not removed, and the relative age relationships of the fracture sets were not presented. Johnson et al. (1965) studied fracture geometries within two formations of significantly different ages, one pre-Laramide and one post-Laramide, in the adjacent Bighorn Basin. The study of Johnson et al. (1965) was designed to test the premise that differences between the fracture patterns within the two lithologies would suggest that a pre-Laramide orogeny had occurred in the Bighorn Basin. Although the study was inconclusive, fracture orientation and length data were collected and interpreted to suggest the mechanism by which each fracture set formed. Two major joint sets were recorded: one trending east–west and one trending between 105° and 155°. Two minor joint sets also were recorded: one trending north–south and one trending between 025° and 065°. The deformation modes of these fracture sets were not interpreted from outcrop observations, but were instead suggested based on angular relationships between fracture sets and fold axes.

In this paper, we present new field data collected at 60 sites across the northwestern half of the anticline that consist of fracture mode (opening or shear) and geometry (orientation relative to bedding, size, and spacing) at the meso- and microscale, along with the chronological relationships among the fracture sets. We focus on the interpretation of these data as an indicator of fold kinematics.

2. Geological and tectonic setting

Sheep Mountain Anticline is located along the eastern flank of the Bighorn basin, which trends NW/SE and is bounded to the east by the Bighorn Mountains, to the south by the Owl Creek Mountains, to the west by the Absaroka and Beartooth Mountains, and to the north by the Nye–Bowler Lineament (Fig. 1). During the Paleozoic and Mesozoic, this basin filled with approximately 3000 m of sediments (Thomas, 1965; Ladd, 1979). The oldest formation exposed at Sheep Mountain is the Lower Carboniferous Madison Limestone (Fig. 3), which is about 200 m thick, and is topped by a paleokarst surface. The Madison Formation is unconformably overlain by the Upper Carboniferous Amsden Formation. The base of the Amsden Fm. is marked by a crossbedded, light gray fine-grained quartz arenite (Ladd, 1979). The remainder of the formation consists of thick siltstones, sandstones, shales and carbonates. Above

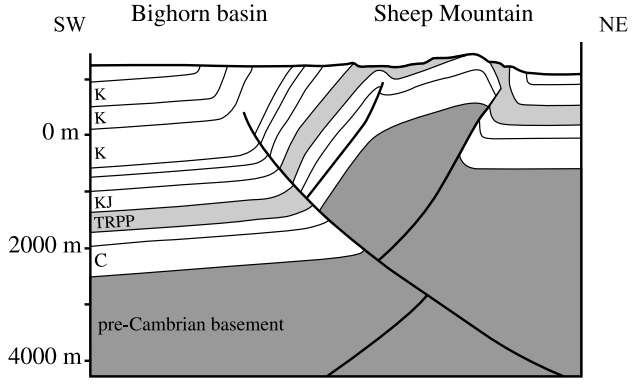

Fig. 2. Cross-section through Sheep Mountain (see Fig. 1b for location) as interpreted by Stanton and Erslev (2004). The fold is asymmetric and underlain by two basement thrust faults: an older NE-verging fault offset by a SW-verging fault (Stanton and Erslev, 2004). The formation above the Cambrian rocks is the Madison Fm. TRPP includes the Amsden (Pennsylvanian), Tensleep (Pennsylvanian), Phosphoria (Permian) and Chugwater (Triassic) Fms; this layer is highlighted in light gray and includes those rocks sampled for fracture analysis. Abbreviations: Cambrian (C), Cretaceous–Jurassic (KJ), Cretaceous (K).

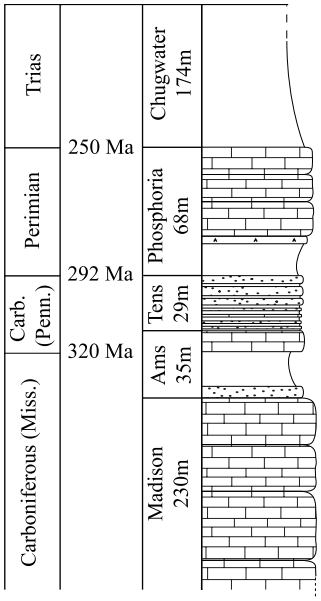

Fig. 3. Stratigraphic section for formations that outcrop at Sheep Mountain (after Ladd, 1979). Abbreviations: Mississippian (Miss), Pennsylvanian (Penn.), Amsden (Ams.), Tensleep (Tens.).

the Amsden Fm., the Tensleep Formation (also Upper Carboniferous in age) is composed of interbedded thin sandstones, shales, and carbonates in its lower part and thicker beds of crossbedded quartz arenite in its upper part. Above the Carboniferous section is the Phosphoria Formation, Permian in age. The lower beds of the Phosphoria Fm. are predominantly siltstones and shales, with a thin interbedded gypsum layer (Ladd, 1979). Higher in section, the Phosphoria Fm. is composed of thick carbonates (biolithite, micrite and biosparite). Due to minor Ancestral Rocky Mountains uplift, the Tensleep and Phosphoria Fms are thinned at Sheep Mountain (Simmons and Scholle, 1990). Above these units, the base of the Mesozoic rocks is defined by the Triassic Chugwater Formation, distinctive due to its red color. The overlying sediments are composed of sandstones and shales that have been eroded in the Sheep Mountain area.

At the end of the Maastrichtian and during Paleocene times, the Laramide orogeny produced a NE-trending compression (Dickinson and Snyder, 1978; Engebretson et al., 1985; Bird, 1998; Bird, 2002). Sheep Mountain anticline formed during the Laramide orogeny as a basement-cored, doubly-plunging, asymmetric fold (Figs. 1 and 2). Given its trend (NW–SE),

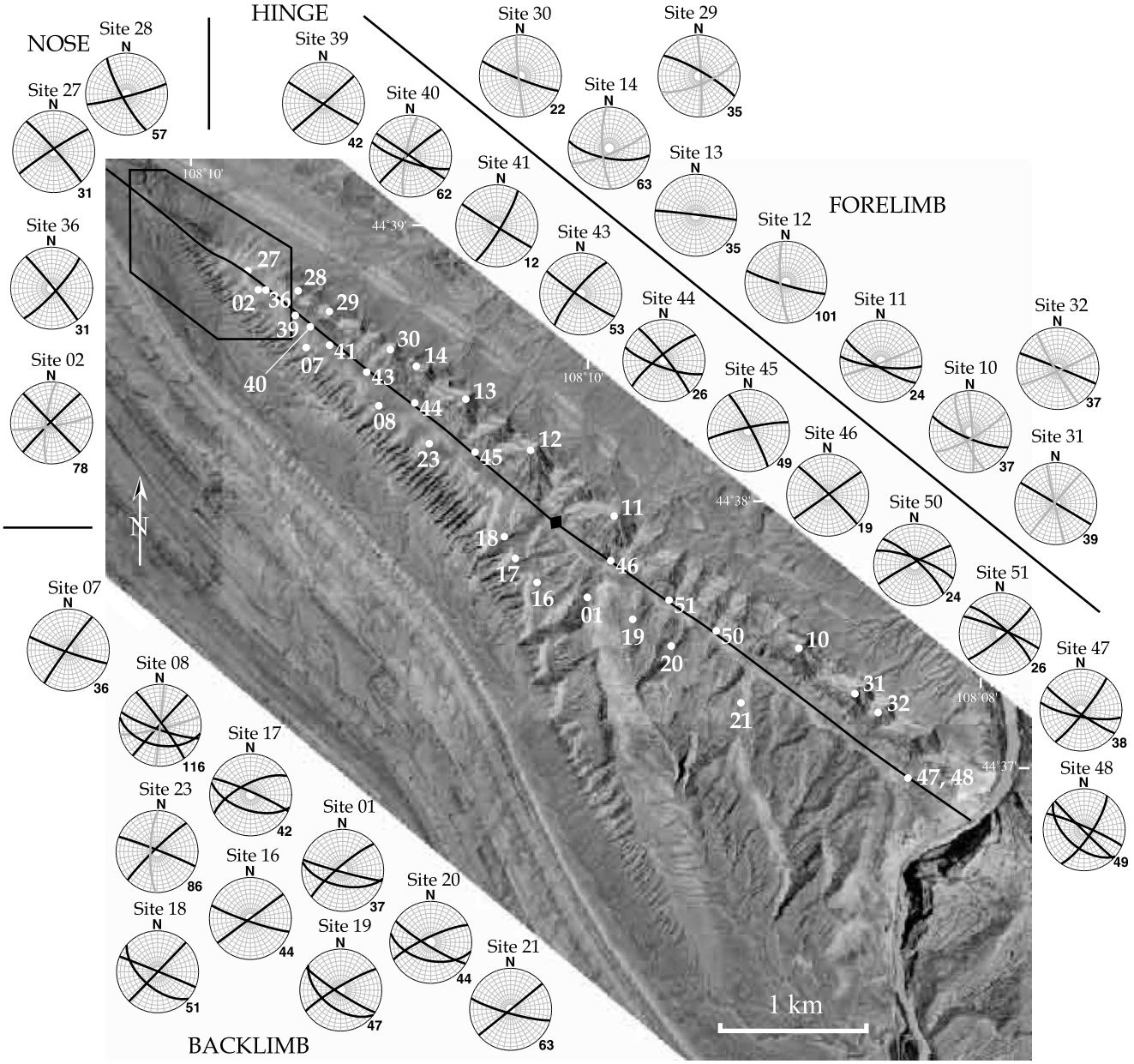

Fig. 4. Aerial photograph of Sheep Mountain with the backlimb, forelimb, and hinge fracture measurement sites and corresponding polar stereonets. Great circles represent the average bedding-corrected orientations of fracture sets (see Section 3.1 for explanation). Black great circles correspond to major fracture sets. Gray great circles correspond to minor fracture sets. These minor fracture sets are not considered in the present analysis of fold evolution. The forelimb contains one abundant systematic set that strikes 110° and is perpendicular to bedding (Set I). The backlimb contains three bedding perpendicular fracture sets: striking 110° (Set I), striking 045° (Set II), and striking 135° (Set III). One set striking 110° is oblique to bedding (Set IV). In the hinge, three fracture sets are bedding perpendicular: striking 110° (Set I), striking 045° (Set II), and striking 135° (Set III). The fractures of Set III are largely restricted to the hinge. Polygon shows location of Fig. 5.

the fold formed perpendicular to the interpreted Laramide direction of compression (NE–SW). This trend is similar to that of many folds within the Rocky Mountains, although others formed at acute angles to the regional compression (Erslev, 1993). At Sheep Mountain, the steep northeastern limb (forelimb) dips between 40° and 90° northeast. This dip is shallower near the fold noses and steeper in the central part of the fold. In the southwestern backlimb, bedding dips are between 10° and 40° southwest. The shape of Sheep Mountain Anticline changes along the fold axis. Near the northern termination, the fold plunges approximately 20° northwest and the profile is very tight. Toward the south, the asymmetry increases while the fold hinge becomes rounder. At the southern termination, the plunge of the fold axis is approximately 10° southwest.

The fold overlies a fault that has been interpreted as a SW-dipping thrust (Hennier and Spang, 1983; Forster et al., 1996; Stanton and Erslev, 2004). Stanton and Erslev (2004) suggested that the displacement along this fault reaches a maximum beneath the central section of the anticline and decreases toward the north and south noses. They conclude that this SW-dipping thrust was later cut by a NE-dipping thrust (Fig. 2). This fault chronology is in opposition to the studies of Hennier and Spang (1983) and Forster et al. (1996), which suggest that the fault responsible for the formation of the Sheep Mountain Anticline is a SW-dipping backthrust of an older NE-dipping thrust, and Stone (2004), which suggests that the SW- and NE-dipping thrusts developed contemporaneously in early Laramide time.

Smaller scale faults and bed-parallel slip with slickensides (Hennier and Spang, 1983), indicate a component of flexural-slip folding with slip directions approximately normal to the fold axis. Additionally, some small reverse faults are present in the hinge and the backlimb of the anticline (Hennier and Spang, 1983; Forster et al., 1996). In the backlimb, a smaller fold branches from the main anticline and has an axis trending NNW–SSE. This structure apparently is related to a shallower thrust fault that is not linked to any basement fault (Hennier and Spang, 1983; Forster et al., 1996; Savage and Cooke, 2004; Stanton and Erslev, 2004).

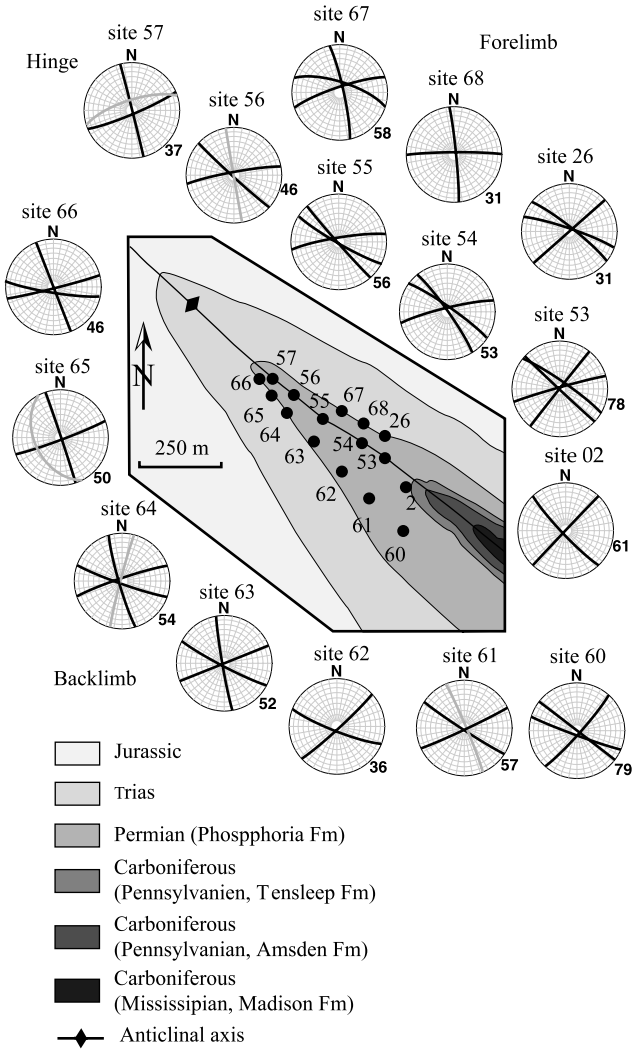

Fig. 5. Geologic map from Rioux (1994) of the nose of Sheep Mountain Anticline with the nose fracture measurement sites and the corresponding polar stereonets. Great circles represent the average bedding corrected orientations of fracture sets measured within the limestone of the Phosphoria Fm. Black great circles correspond to the major fracture sets. Gray great circles correspond to minor fracture sets.

3. Methods

3.1. Fracture sampling

Fracture populations (Figs. 4–6) were sampled only in the part of the anticline north of the Bighorn River because, to the south, both access to and exposure of fractured pavements are poor. Sandstones were sampled from the Tensleep Fm. in the

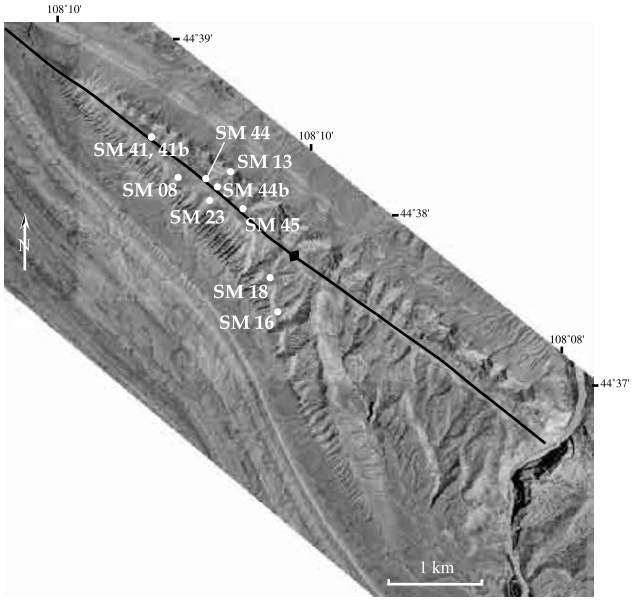

Fig. 6. Sample sites for microscopic analysis. Samples SM08, SM13, SM16, SM18, and SM23 are from the Tensleep Fm. Samples SM41, SM44, and SM45 are from the Amsden Fm. All sites correspond numerically to sites shown in Fig. 4.

anticlinal limbs and from the Amsden Fm. in the hinge. The limestone of the Phosphoria Fm. was sampled in the fold nose to increase data coverage and to assess fracture development as a function of lithology. Fracture orientation, length, spacing, and mode of deformation (opening or shearing) were recorded, as were abutting relationships, evidence for fracture reactivation and evidence for fracture infilling. Spacing measurements are parallel to the bedding and are not normalized to bed thickness. At each station, all fractures were sampled in areas typically a few tens of meters on a side.

The data presented here include images of thin sections cut perpendicular to fracture strike (Fig. 6). The samples were collected at the same sites where fracture orientations were measured, and thin section observations were used to confirm the mesoscopic determination of deformation mode. When the mode is ambiguous, the structures are called fractures, where confirmed they are referred to as joints (opening) or shear fractures. We collected several samples for each set of fractures in each structural position on the fold. Thus, we believe that the samples are representative of the deformation modes observed throughout the northern part of the anticline. For brevity, we show only a few typical thin sections.

3.2. Data processing

Four fracture sets are defined based on both orientation data and deformation mode. Where evidence of tail cracks or extensional jogs can be observed in the field, or where crushed or aligned grains along fracture walls can be observed in thin section, the fracture is determined to have had a shearing mode of deformation. Where hackle marks are observed along fracture walls in the field, or where veins of large, euhedral calcite crystals can be observed in thin section, the fracture is determined to have had a tensile mode of deformation. Members of a fracture set share both a common range of strike and dip orientation and, with the exception of Set I, a common deformation mode. With one exception, common orientation can be identified only after removal of bedding dip by stereographic rotation. Fold plunge was not removed because it is less than 20° and it does not significantly affect orientation. Commonality of fracture orientation after removal of bedding dip, where the fractures are subparallel and bed perpendicular, is taken as supportive of a prefolding origin (Hancock, 1985). Fracture strikes either perpendicular or parallel to bedding strike are not affected by rotation of bedding to remove the dip and may be interpreted as occurring during any stage of fold growth. We present stereonets of the orientation data at each measurement site that are not weighted by abundance, as we believe that this can be biased by outcrop conditions. However, we note when a fracture set is less systematic (less planar, parallel, and horizontally and vertically through-going) and less abundant than others.

The stereonets presented in this paper were generated with a prototype computer code developed in the Structural Geology Department of the Institut Français du Pétrole using an original method for the automatic definition of fracture clusters. Each fracture is represented as a plane with an orientation given by the unit normal vector as a point (pole) on the unit sphere. The density of fractures is estimated at each point on this sphere using an Epanechnikov kernel. Outliers (non-recurring fracture orientations) are removed by filtering, and the density distribution is smoothed by manually changing the variance of the kernel (Wollmer, 1995). In a first step, cluster centers are identified by searching for local maxima of the density map using the method introduced by Kittler (1976). This step results in the definition of a number of fracture sets and a guess for the mean pole of each set. This guess allows each fracture to be classified probabilistically using its distance from each cluster center. Then the algorithm presented by Marcotte and Henry (2002) is used to finalize the fracture classification. This method is based on the assumption of a bivariate normal distribution of fractures within a set. The results of this analysis are presented in a polar stereonet using the Lambert projection on the lower hemisphere with great circles representing the mean plane of each fracture set (Figs. 4, 5, 8–11, 14, and 16–18). In Figs. 8, 10, 11, 14, and 16–18, the polar stereonets depict, from left to right: fractures in present-day orientations (the bedding pole is a bigger dot than the fracture poles on the stereonet), fractures in pre-folding orientations, and the great circle of the calculated mean orientation of the fracture sets.

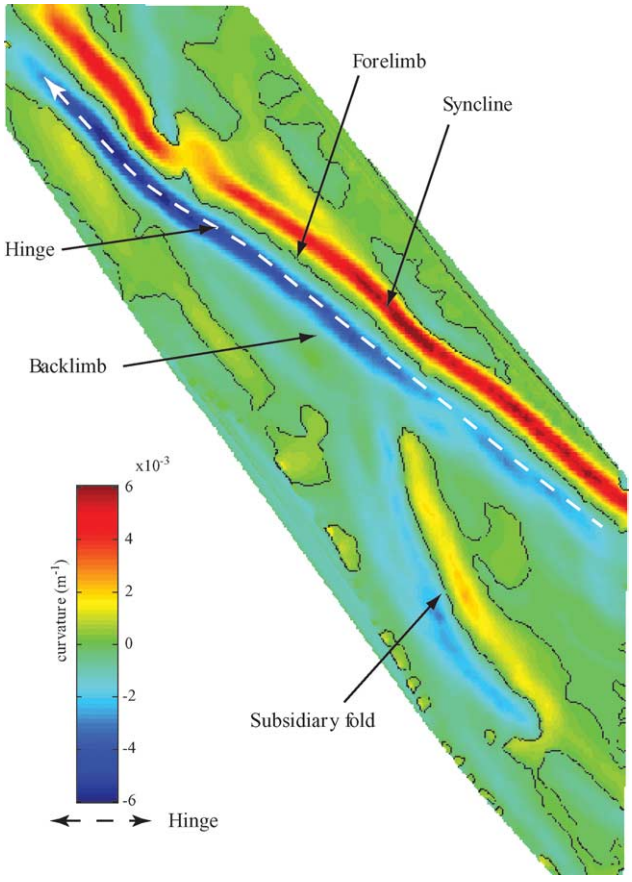

Fig. 7. Curvature map for Sheep Mountain Anticline calculated from the structure contour map in Forster et al. (1996). See text for calculation details. Hot colors represent synclinal curvature and cool colors represent anticlinal curvature.

3.3. Curvature calculation

We computed a curvature map (Fig. 7) to assess the relative curvature of various fold locations. Forster et al. (1996) published a structure contour map of a reference horizon at the base of the Jurassic Sundance Formation. We assume that changes in formation thicknesses across the fold between the Upper Carboniferous Amsden Fm. and the Sundance (about 300 m) are not substantial and therefore that this map can be used to study layers that are stratigraphically below the Sundance from the Amsden to the Permian Phosphoria Fm. (Fig. 3). The structure contour map was generated through field mapping and the construction of serial cross-sections that predict the elevation of the formation in areas where it has been eroded. We digitized the structure contour map and calculated the maximum curvature across the resulting three-dimensional surface using gOcad, a 3D geomodeling software program (Mallet, 2002). The algorithm for maximum curvature selects the principal curvature with the greater absolute value and plots that curvature with its sign. Thus, positive curvature (concave upward) may be differentiated from negative curvature (concave downward). In Fig. 7, zones of hot colors have positive curvature and mark synclinal hinges, whereas zones of cool colors have negative curvature and mark anticlinal hinges.

4. Structural data

4.1. Northeast forelimb

We observe one systematic fracture set, trending 110°, in the forelimb within the Tensleep sandstone after removal of bedding dip (Fig. 4, sites 10–14 and 29–32). From abutting relationships in other structural positions of the fold (see Section 4.2), this set is interpreted as the first formed in the area, and is thus called Set I. Additionally, non-systematic sets are locally developed (striking primarily 070° and 180°, Fig. 4), but are interpreted to reflect local rather than fold-scale or regional deformation, and so are not considered further (Fig. 4).

Set I fractures are linear and several meters long (Fig. 8). Their spacing is on the order of a few tens of centimeters. In the field, their deformation mode is difficult to determine, as different fractures within the set exhibit characteristics of either joint or shear band morphology. In some cases, the fractures are open with or without mineral fillings, and in other cases they stand up from the outcrop with small positive relief. This latter attribute may be related either to cementing (for the case of joints or dilational bands) or tighter packing of grains within the fracture (for the case of deformation bands). At the microscale, the fractures are defined by zones that contain smaller quartz grains with more angular shapes, poorer sorting, lesser porosity, and smaller calcite cement crystals than the surrounding rock (Fig. 9). These features are characteristic of deformation bands (Aydin, 1978; Antonellini et al., 1994), and we interpret some Set I fractures to be such brittle structures. However, no offset or sense of shearing was detectable either in

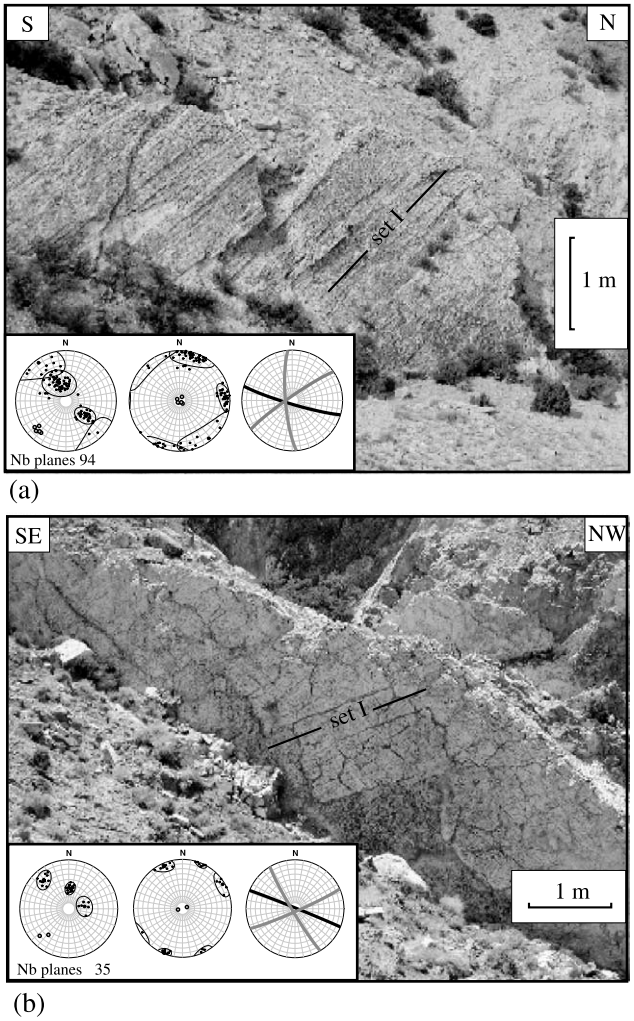

Fig. 8. Field photographs of fracture patterns on tilted bedding surfaces taken at forelimb sites 12 (a) and 32 (b). Note the abundance and small spacing of Set I fractures (striking 110°). Numerous fractures with different orientations are non-systematic. Polar stereonets left to right are present day fracture poles, pre-folding fracture poles, and great circles for mean orientations of each set. Poles to bedding are heavy circles.

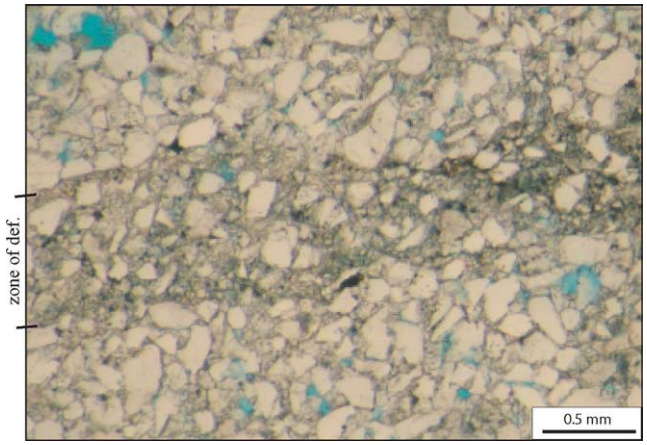

Fig. 9. Microscopic detail of a Set I fracture in the forelimb from site SM13. The deformed zone has less porosity and more calcite cement than the surrounding host rock. The zone also contains more angular quartz grains that are mostly smaller than grains in the host rock.

thin sections or in the field. Thus, we are unable to identify a deformation mode for these fractures.

Bed-normal reverse faults that strike 110° and dip 30° south are present along the forelimb (at sites 11, 13, 14, and 30–32 on Fig. 4, and see Fig. 10). The faults are oblique to the fold axis and to the Laramide regional compression. The striations noticeable along the fault surfaces indicate oblique slip, consistent with the resolution of shear stress from the NE directed compression onto these planes (Fig. 10).

4.2. Southwestern backlimb

In the backlimb, four fracture sets are observed in the Tensleep sandstone (Fig. 4, sites 1, 7, 8, 16–21, and 23). After removal of bedding dips, three of these sets strike 110°, 045°, 135° and are perpendicular to bedding, whereas one set strikes 110° and is nearly vertical (not perpendicular to bedding).

Bed perpendicular fractures trending 110° (Figs. 4 and 11) are correlated to Set I fractures in the forelimb. These fractures are 10–20 m long as compared to a height of a few meters (equivalent to bed thickness). The fracture traces are linear and their spacing varies from 1 to 3 m. They lack tail cracks, Riedel fractures, or other shearing-related secondary structures (Pollard and Aydin, 1988). As in the forelimb, their deformation mode is difficult to determine in the field. They resemble joints at some sites and at other sites resemble deformation bands. Microscopically, Set I fractures are characterized by a decrease of grain size, a decrease of porosity, and an increase in amount of calcite cement as compared to the host rock (Fig. 12). These fractures show no kinematic evidence of shearing.

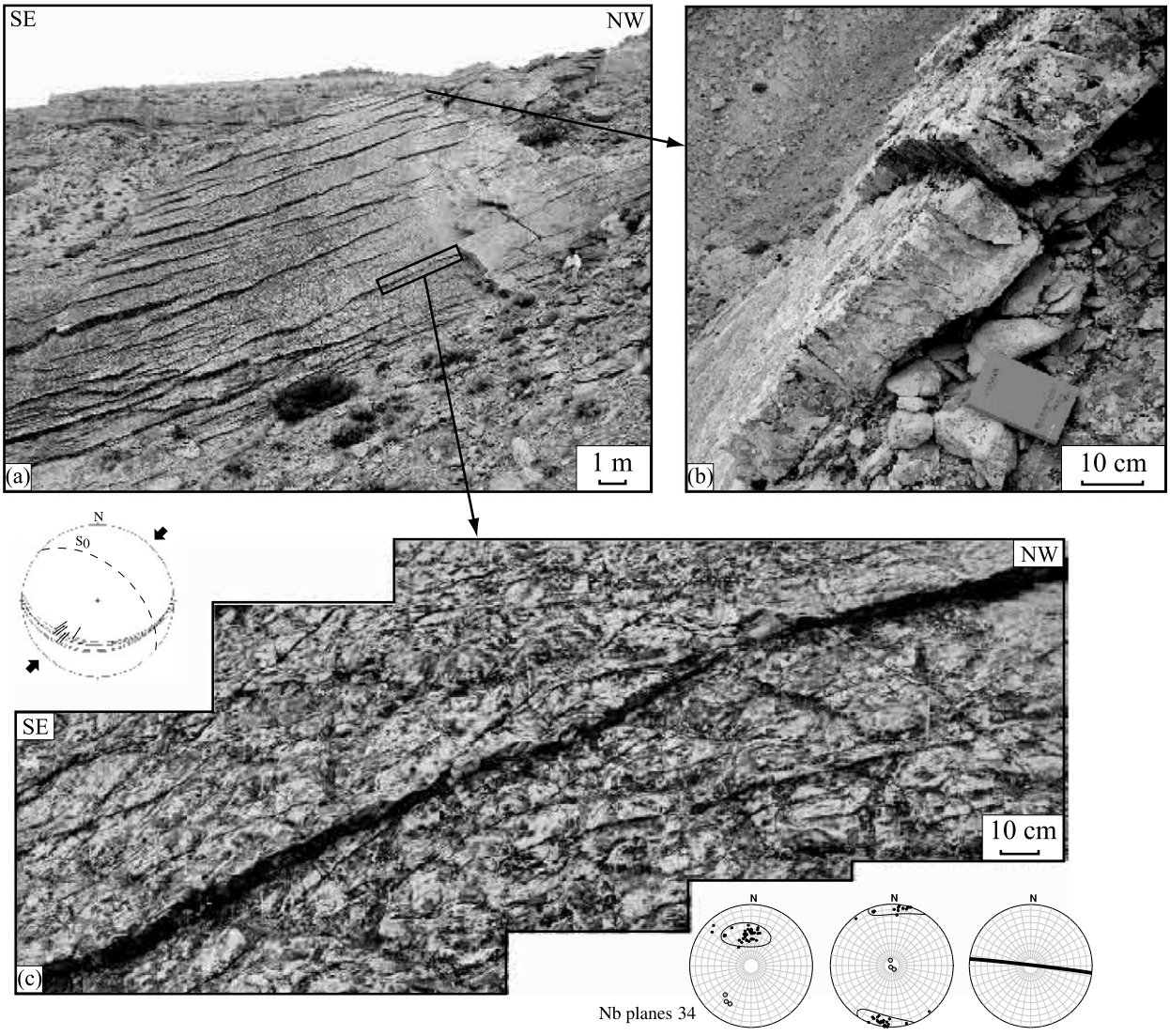

Fig. 10. Reactivated Set I fractures in the forelimb. (a) Field photograph of small reverse faults offsetting a sandstone bedding surface of the Tensleep Fm. at site 13. (b) Cross-sectional view of the sandstone bed in (a) showing offset. (c) Close up of one fault on a bedding surface. (d) Striation data (thin arrows on the fault planes) indicating oblique reverse slip along the faults. The large arrows are inferred direction of compression that is compatible with the striations. Polar stereonets left to right are present day fracture poles, pre-folding fracture poles, and great circle for mean orientation of set. Poles to bedding are heavy circles.

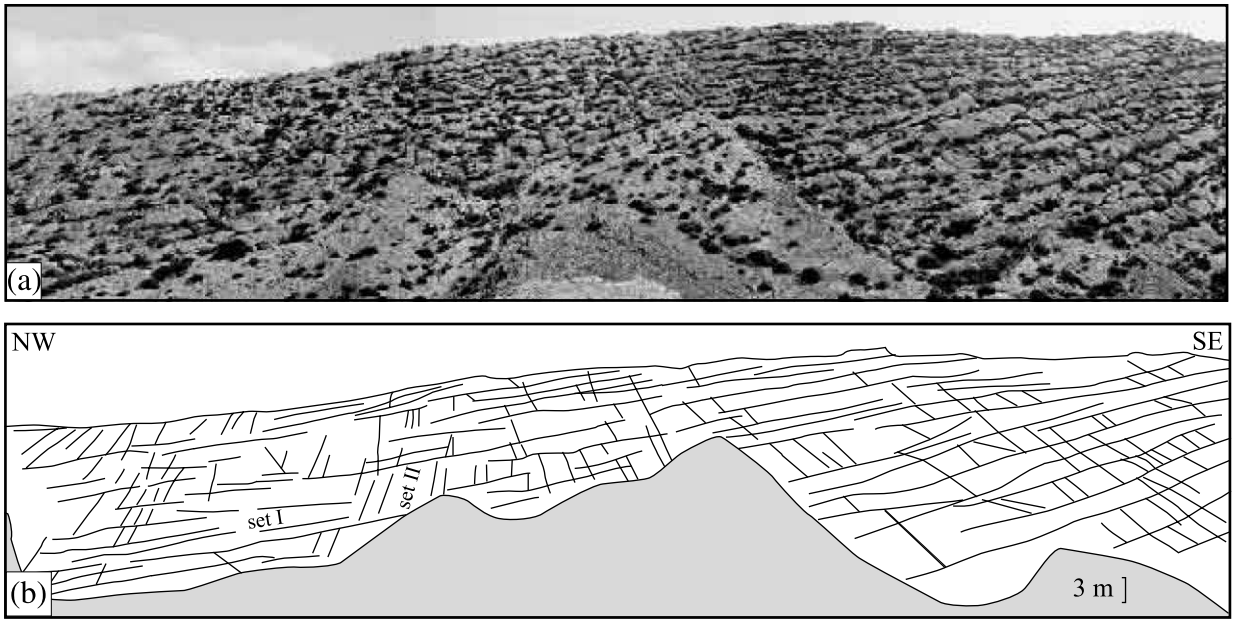

Fig. 11. Fracture pattern in the backlimb. (a) Field photograph at site 8 in the Tensleep sandstone. (b) Line drawing of the outcrop in (a) that shows Set II fractures (strike of 045°) terminating at Set I fractures (strike of 110°).

Set II fractures trend 045° (Figs. 4 and 11) and are bed perpendicular. Set II fractures terminate against Set I fractures (Fig. 11) and, as a result, are only 2–5 m in length. Their traces are linear and their spacing is approximately 1 m. In the field, they have purely strike-perpendicular offset indicating an opening mode of deformation. As seen in thin section, the fillings typically consist of large calcite crystals without evidence of grain fracturing or crushing, which supports a dilational origin (Fig. 13a).

Set III fractures have a more restricted occurrence than Sets I and II (Fig. 4, sites 18–20 and 52). They trend 135°, are bed perpendicular, and contain a coarse calcite mineral filling (Fig. 13b) that is indicative of opening mode. The length of these fractures is on the order of a few meters. The termination relationships with other fracture sets are difficult to determine because of the small number of these fractures. Age relationships are more easily determined from observations within the fold hinge, where fractures with a similar orientation are more numerous.

Set IV fractures trend 110° and are parallel to Set I fractures, but are vertical and therefore oblique rather than perpendicular to bedding (Figs. 4 and 14). Abutting relationships are difficult to establish because they have been observed mainly in cross-section, which reveals only their vertical dip. These fractures are several meters long with an approximate spacing of 1 m. In the field, most Set IV fractures are open, and all lack evidence of shearing. Microstructural examination shows that the preserved calcite filling is distinct from that in Set II and Set III fractures (Fig. 13c). Matrix grains at the walls of Set IV fractures are crushed and display a preferred elongation direction, suggesting a two phase deformation: a shearing event followed by a tensile vein filling event.

4.3. Hinge

In the hinge, fracture measurements were made in sandstone beds of the Amsden Fm. (Fig. 4). We observed three sets of fractures with orientations: 110°, 045°, and 135° (Fig. 4, sites 39–41, 43–48, 50, and 51), which we correlated to sets identified in the forelimb and backlimb.

Set I fractures trend 110° and are bed perpendicular. They are less numerous in the hinge than in the limbs, and their spacing is greater. In thin section (Fig. 15a), these fractures are

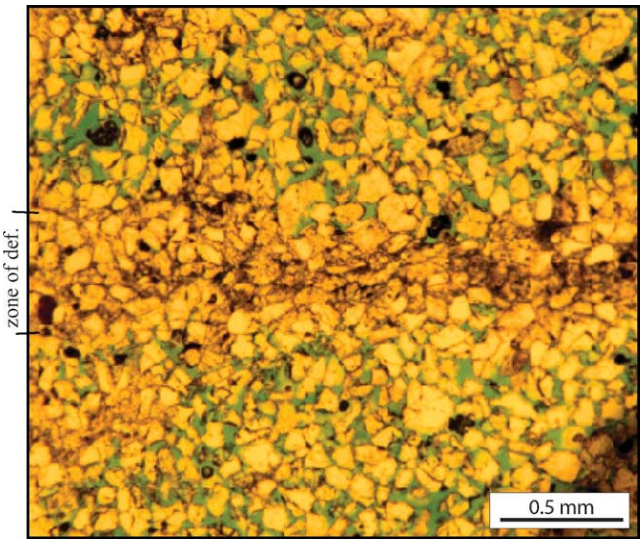

Fig. 12. Microscopic details of a set I (110°) fracture in Tensleep Fm. sandstone of the backlimb at site SM16. The fracture is characterized by a zone with less porosity, smaller quartz grains and a larger amount of calcite cement as compared to the host rock.

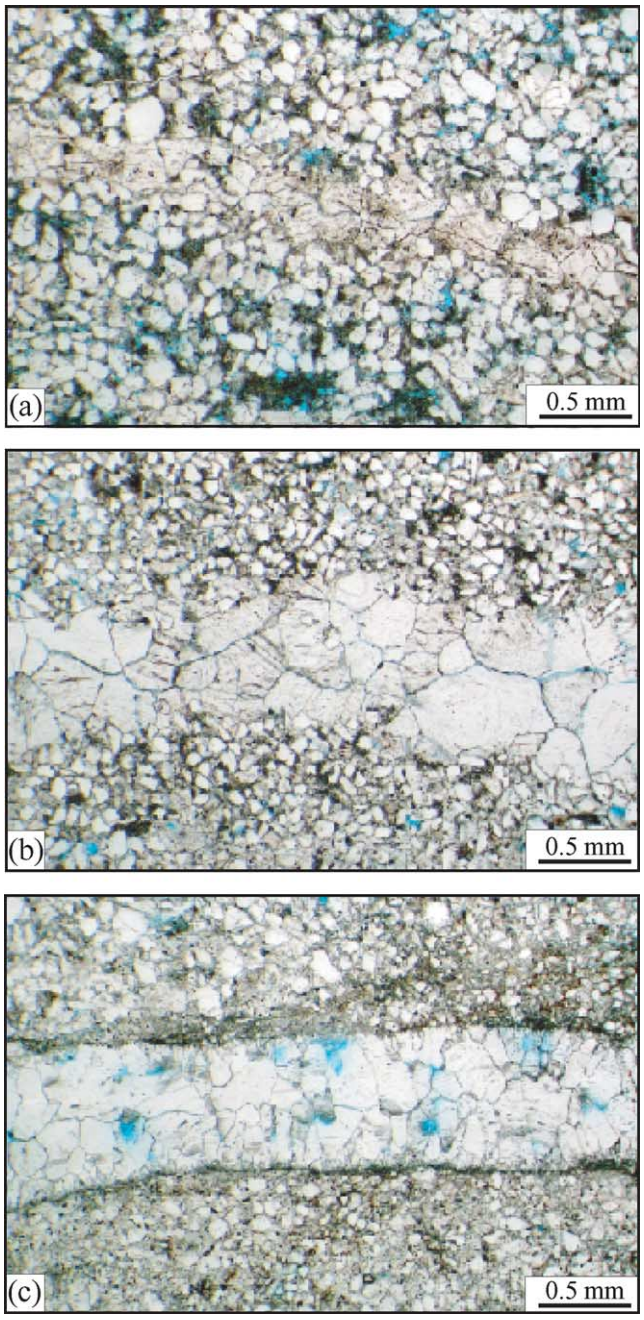

Fig. 13. Microscopic detail of fractures in the Tensleep Fm. sandstones of the backlimb. These photomicrographs all show structures with distinct fracture walls and a large-crystal calcite filling. (a) Microscopic structure of a Set II (045°) fracture at SM8. (b) Microscopic structure of a Set III (135°) fracture at SM23. (c) Microscopic structure of a Set IV (110°) fracture at SM18. In addition to the characteristics seen in (a) and (b) there are very fine grains along the fracture walls.

marked by reduced grain size and porosity as compared to the host rock, similar to the Set I fractures in the forelimb (Fig. 9). The alignment of elongate grains seen in these thin sections is indicative of shearing deformation. This set is identified at 6 out of 11 locations on the hinge including sites 40, 44, 47, 48, 50, and 51 (Fig. 4).

Set II fractures trend 45°, are bed perpendicular, and have a coarse calcite filling similar to that seen in Set II fractures in the backlimb (Figs. 4, 15b, and 16). These fractures are joints, with lengths of a few meters and 1 m spacing.

Set III fractures trend 135° (parallel to the fold axis), are bed perpendicular, and are observed primarily in the hinge. For the majority of the abutting relationships in the hinge, Set III fractures end on, and thus postdate, Set II fractures (Fig. 16). Set II fractures abut Set I fractures in the backlimb, so we infer that Set III fractures also postdate Set I fractures.

4.4. Northern nose

The fold nose is defined as the area NW of the position in the backlimb where, due to the fold shape, bedding strike has rotated to 150° from the typical value of 135° elsewhere along the limbs (Fig. 4). This change in orientations occurs near site number 39 in Fig. 4, and is visible on the air photo where the bedding traces of layers turn clockwise as one proceeds from the backlimb to the nose. In the nose, fracture data were collected primarily from limestones within the Phosphoria Fm. because outcrops of the Tensleep Fm. are limited (Figs. 4 and 5). Outcrops of both the Tensleep and Phosphoria Fms are present at the southern extent of the nose, and we compare measurements from these two formations to determine similarities and differences between fractures within the two lithologies. The comparison was done at sites 2, 27, and 36 in the Tensleep Fm. (Fig. 4) and sites 2 and 60 in the Phosphoria Fm. (Fig. 5).

In the nose hinge, as described earlier, the fractures in the Tensleep Fm. consist of two main joint sets trending 045° (Set II) and 135° (Set III) (Fig. 4, sites 2, 27, and 36, and Fig. 17). From abutting relationships, Set II joints predate Set III joints (Fig. 16). In the nose hinge, we also observe two main fracture sets in the Phosphoria Fm. (Fig. 5, site 2). One set is NE-trending and composed of joints (Fig. 5, site 2, and Fig. 18). Another set is SE-trending (Fig. 5, site 2, and Fig. 18) and also composed of joints. The chronology is difficult to determine (Fig. 18) as the abutting relationships are not entirely consistent: in some cases the NE-trending set stops on the SE-trending set, and in other cases the SE-trending set stops on the NE-trending set. However, based on strike and mode of deformation, we suggest that these two joint sets are similar to Sets II and III described throughout the fold.

Fractures in the backlimb (Fig. 4, site 7) are similar in terms of deformation mode to the fractures in the nose backlimb (Fig. 5, site 60). Fractures in the forelimb (Fig. 4, site 29) also are similar to the fractures in the nose forelimb (Fig. 5, site 26). The common occurrence of both Set II and Set III in the sandstones and limestones at the selected sites is used to infer that fracture data recorded within the limestones is a reasonable proxy for the fracture pattern that exists within the buried sandstone beds of the fold nose.

We observe across the nose that the NE-trending Set II joints vary in orientation from 045° to 070° toward the nose (Fig. 5). Fractures trend 045° at sites 2, 26, 53, and 60, and 070° at all but one of the remaining sites. The SE-trending Set III joints also vary in orientation throughout the nose, but to the largest extent within the nose backlimb (Fig. 5). They trend

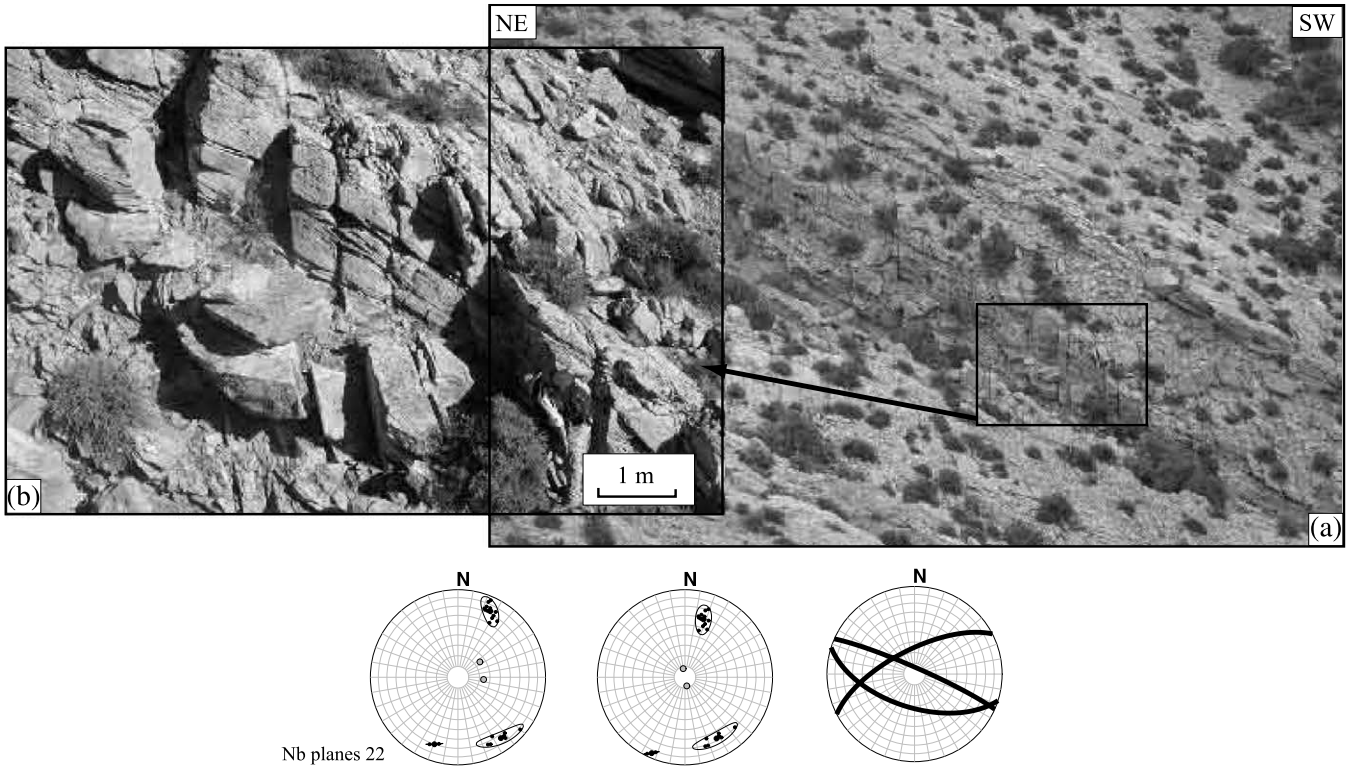

Fig. 14. Vertical Set IV fractures in the backlimb. (a) Field photograph of Set IV (110°) fractures at site 23 in Tensleep sandstone. (b) Close-up photograph. These fractures do not show any evidence of shearing. Polar stereonets left to right are present day fracture poles, pre-folding fracture poles, and great circles for mean orientations of each set. Poles to bedding are heavy circles.

135° at sites 60, 61, and 62, and trend 160° at sites 64, 65, and 66. In the nose hinge, these SE-trending joints maintain an average orientation of 140° at all sites except site 57 (Fig. 5).

Set I fractures are less abundant in the nose than in the limbs. They are observed at sites 26, 53–55, 60, 62, 64, 66, and 67 (Fig. 5).

5. Interpretation

The four fracture sets found at Sheep Mountain anticline provide qualitative constraints for the temporal and spatial evolution of deformation of the sedimentary layers within the anticline. The following discussion synthesizes field and thin-section observations first to present an interpretive chronological history of fracture development and then to make inferences about fold kinematics.

5.1. Pre-existing fractures

Set I fractures are observed in three-quarters of the locations across the fold and are systematically perpendicular to bedding. The deformation mode of these fractures remains uncertain (see previous sections and Figs. 9, 12, and 15a and b) because we do not know if they initiated with shearing (e.g. as deformation bands) or with opening (as joints) and subsequently were sheared.

Set I is oblique to the trend of the fold, striking approximately 25° counterclockwise from the fold axis. Additionally, abutting relationships indicate that Set I predates all other fracture sets. Thus, we interpret Set I as the oldest set and as having initiated prior to the Laramide orogeny (Fig. 19). A similar interpretation was made by Silliphant et al. (2002) at Split Mountain in Utah and Hennings et al. (2000) at Oil Mountain in Wyoming, where a fracture set of similar strike (WNW-trending) is present at nearby locations where bed dips are approximately horizontal, as well as in each structural position of the fold after rotation of the bedding to horizontal.

Fractures, striking 110° when bedding is restored to horizontal, and dipping perpendicular to bedding, also are found regionally near Sheep Mountain in the Black Hills of western South Dakota and northeastern Wyoming (Wicks et al., 2000). In this location, the fracture set was interpreted to predate Laramide compression. Conversely, a set of fractures of this orientation was found near the Tensleep fault in the Southeast Bighorn basin (Allison, 1983) and was interpreted as a late joint set. The chronology in that case was deduced from a statistical analysis of the number and scatter of joint measurements, however, and not from abutting relationships observed in the field.

In other places in Wyoming and Montana, fractures subparallel to Set I have not been observed: for example at Elk Basin in Montana (Engelder et al., 1997), at Garland and Little Sand Draw in the southeast Bighorn Basin (Garfield et al., 1992), and at Teapot Dome (Allison, 1983; Cooper et al., 1998). This suggests that Set I did not develop uniformly across the region. Similarly, at Sheep Mountain, Set I fractures are present primarily within the limbs, and are less abundant within the hinge and the nose. One explanation is that this fracture set

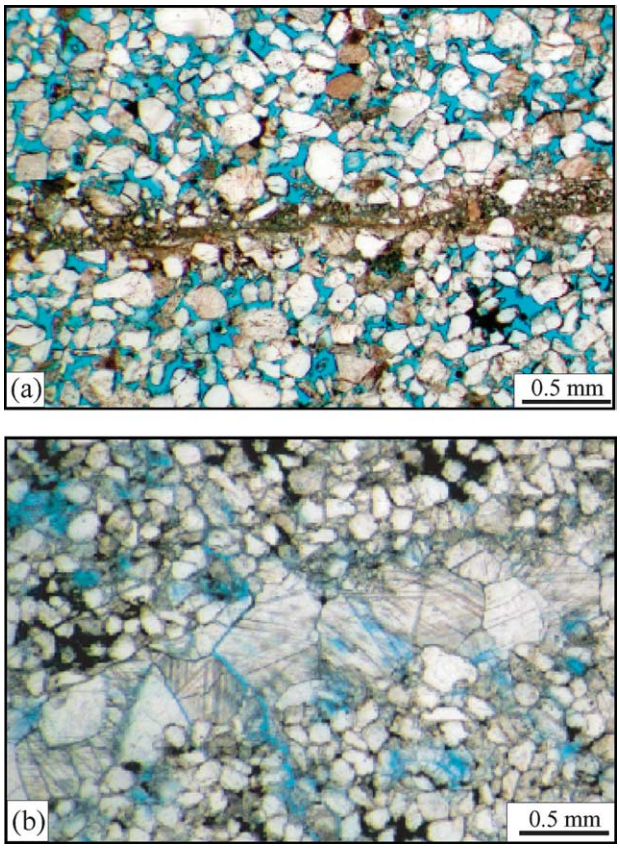

Fig. 15. (a) Microstructure of a Set I (110°) fracture in a sandstone of the Amsden Fm. in the hinge at site SM44. The fracture is composed of crushed matrix grains surrounded by quartz cement. (b) Microstructure of a Set II (045°) fracture in sandstone of the Amsden Fm. in hinge at site SM41. The fracture has distinct walls and is filled with large crystals of calcite cement.

did not develop homogeneously, but was less well developed within patches in a given layer, due to subtle differences in diagenesis or stress state. Another explanation is that this fracture set is not well developed in limestone (the dominant formation cropping out in the nose) due to material properties differing from those of the sandstone and/or to higher position in the stratigraphic column. Sets II and III, however, are expressed both in the Tensleep Fm. and in the Phosphoria Fm.

5.2. Early Laramide compression: onset of faulting and folding

Set II joints strike parallel to the NE–SW direction of Laramide compression (Dickinson and Snyder, 1978; Engebretson et al., 1985; Bird, 2002) and are perpendicular to bedding. We have deduced that Set II joints predate the fold-parallel hinge-restricted Set III joints. Thus, we interpret Set II joints to have formed in response to early Laramide compression, prior to significant development of the fold (Fig. 19).

Joints initiating parallel to the maximum compression direction of a tectonic stress are documented in the literature (e.g. Engelder and Geiser, 1980; Engelder et al., 1997). Joints with the same orientation as Set II (after removal of bedding dips) are found in several locations near Sheep Mountain: at Garland and Little Sand Draw in the southeast Bighorn Basin (Garfield et al., 1992), at Teapot Dome in Wyoming (Allison, 1983; Cooper et al., 1998) and in the southeast Bighorn Basin near the Tensleep fault (Allison, 1983), confirming their regional status. Additionally, pressure-interference tests for seven reservoirs in the Bighorn Basin revealed consistent permeability anisotropy in the NE direction (Haws and Hurley, 1992), supporting our interpretation of Set II as a regional fracture set. At Sheep Mountain, we find Set II joints in the backlimb, the hinge, and the nose (Figs. 4, 5, and 19). Fractures of this set are much less numerous in the forelimb, however, suggesting that an early structure, most likely the incipient fold or the underlying thrust fault, may have influenced their distribution (Fig. 19) (Bellahsen et al., 2006).

Sheep Mountain Anticline is interpreted as a fault-related fold associated with a blind thrust fault that dips around 50° SW (Stanton and Erslev, 2004). Slip along this thrust would induce a zone of enhanced compression above the fault tip (Bellahsen et al., 2006). We suggest that such a stress perturbation inhibited the formation of Set II fractures in the rocks corresponding to the forelimb during folding.

Field evidence supports the interpretation that Set II fractures predate all fracture sets except Set I and, thus, they predate the hinge-parallel Set III joints that are inferred to be fold related. Yet, these timing relationships do not require Set II to be pre-folding. Set III may have initiated during a later stage of the fold evolution rather than at the onset of folding. In this case, Set II joints could have formed after the beginning of fold evolution but before the development of Set III.

Thus, we suggest a regional deformation was responsible for Set II fractures and that the paucity of Set II joints in the forelimb of Sheep Mountain Anticline is due to a stress perturbation resulting from slip on the underlying basement thrust fault (Bellahsen et al., 2006). The rotation in strike of Set II fractures in the nose is most likely also related to stress perturbations from the underlying fault. As the orientation perturbation is found only in the present nose, the underlying fault would have established its strike-parallel dimension early in its development. This concept has been documented for faults in extensional domains (Walsh et al., 2002) and inferred for faults in compressional domains (Julian and Wiltschko, 1983; Armstrong and Bartley, 1993; Fischer and Christensen, 2004). Such a mechanism is usually explained by invoking fault reactivation (Walsh et al., 2002). Reactivated faults do not grow laterally until their slip reaches a sufficient value in comparison to length to trigger lateral propagation. The interpretation of the underlying basement fault at Sheep Mountain as reactivated is consistent with previous studies elsewhere in the region (Simmons and Scholle, 1990; Ye et al., 1996).

5.3. Fold growth: intermediate stage

In the hinge, joints striking parallel to the fold axis and dipping perpendicular to bedding are classified as Set III fractures. As previously noted, they could have formed at any

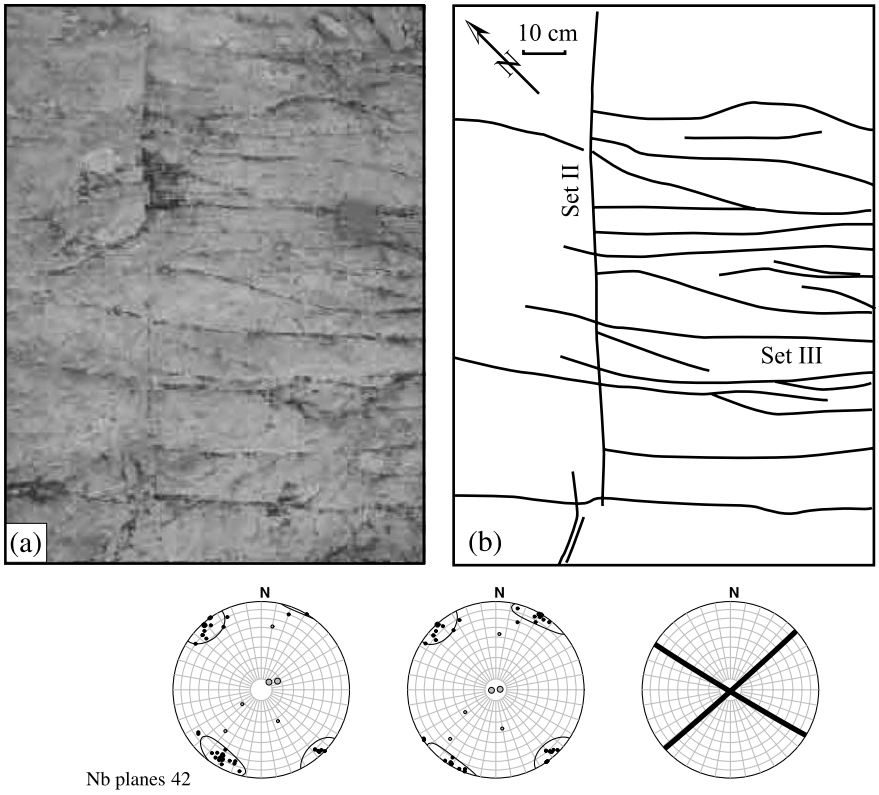

Fig. 16. Fracture pattern in the hinge. (a) Field photograph of bedding surface showing the abutting relationships between Sets II (045°) and III (135°) at hinge site 39 in a sandstone of the Amsden Fm. (b) Line drawing of the outcrop in (a) showing that 8 of 13 Set III fractures terminate at Set II fractures. Polar stereonets left to right are present day fracture poles, pre-folding fracture poles, and great circles for mean orientations of each set. Poles to bedding are heavy circles.

time during folding (Fig. 19). Despite this ambiguity in timing, the concentrated occurrence of these joints in the hinge is consistent with a fixed-hinge model of fold evolution (Allmendinger, 1982; Fischer et al., 1992; Fisher and Anastasio, 1994; McConnell, 1994). Had the hinge migrated, we would expect to find hinge-parallel joints in one or both fold limbs.

We do find some Set III hinge-parallel joints in the backlimb (Fig. 4, sites 18–20). These joints may relate to areas where layer curvature is greater (Fig. 7). The hotter colors of the curvature plot represent areas of tight anticlinal folding. Looking across the anticline in a direction normal to bedding strike, in the northwest, zero or near zero curvature values exist just a short distance from the fold hinge, whereas further southeast this distance is greater. The occurrence of Set III joints in the backlimb increases toward the southeast, where the fold shape changes from tight to a more rounded profile (Fig. 7). This supports our hypothesis that there is a link between curvature and the existence of Set III joints. Where the hinge is tight in the northwest, the limbs are approximately planar and Set III is confined to the hinge.

Set III joints also are found in the fold nose. In the backlimb of the nose, the joint strike changes along the fold from 135° to 160° (Fig. 5). This change roughly coincides with the change in fold limb orientation, as the strike of the layers changes from 130° to 150°, to the northwest of site 39 (Fig. 4) and site 60 (Fig. 5). In the nose portion of the hinge zone, Set III is the main joint set, where it most likely initiated due to layer curvature. The variation in fracture orientation within this set suggests that the length of the fold was set early in fold development, which is consistent with the proposed geometric history of the underlying thrust fault. Analogous changes of Set III joint strike are absent along the more cylindrical part of the fold.

5.4. Fold growth: late stage

During the later stages of fold growth we infer that the fracture patterns in the hinge and in the nose did not change significantly, although some additional fold-parallel joints may have formed. In the limbs, however, new fractures initiated and others were reactivated (Fig. 19).

In the forelimb, we observe small thrust faults with oblique slip (Figs. 10 and 19). They are reverse faults that strike 100° and dip approximately 30° from the horizontal, perpendicular to bedding. Given the geometric similarities to Set I, these structures are interpreted as reactivated Set I fractures. We infer that the reactivation occurred late in the fold evolution. Incorporated into this interpretation is the assumption that Set I fractures rotated passively with the strata and were reactivated when they reached an orientation relative to horizontal that was shallow enough to allow a thrust offset along them.

Set I fractures also could have been reactivated earlier during fold growth. In some kinematic models of fault-propagation folding, thickening and thinning of the forelimb occurs (Jamison, 1987; Chester and Chester, 1990; Erslev,

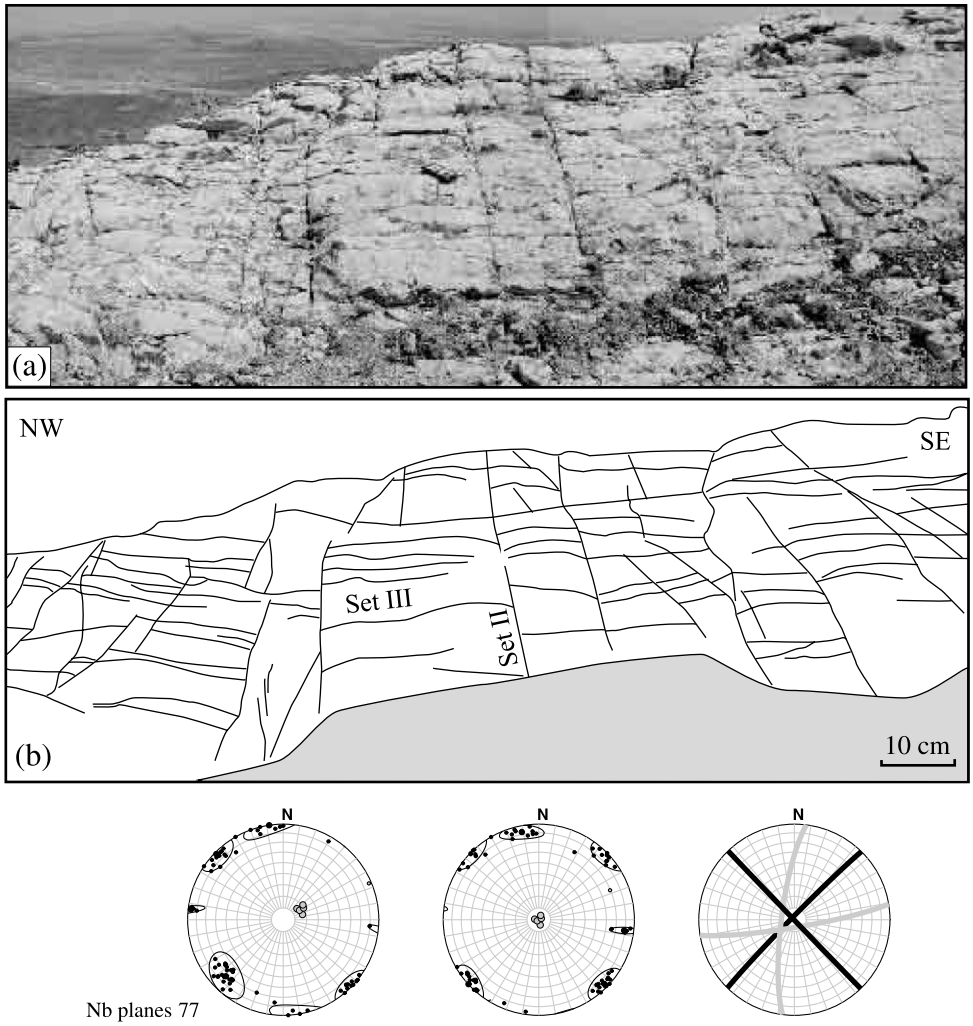

Fig. 17. Fracture pattern in the hinge of the fold nose. (a) Field photograph showing the fracture pattern in a sandstone of the Tensleep Fm. at site 2. (b) Line drawing of the outcrop in (a) showing that Set III (135°) fractures predominantly terminate at Set II (045°) fractures. Polar stereonets left to right are present day fracture poles, pre-folding fracture poles, and great circles for mean orientations of each set. Poles to bedding are heavy circles.

1991; McConnell, 1994; Frizon de Lamotte et al., 1997; Hardy and Ford, 1997; Storti et al., 1997; Allmendinger, 1998; Grelaud et al., 2000). This thinning is apparent on cross-sections shown by Stanton and Erslev (2004). The presence of the reverse faults in the forelimb of Sheep Mountain would be consistent with such forelimb deformation.

Stanton and Erslev (2004) suggested that the thrust fault that created Sheep Mountain anticline was cut by a later NE-dipping thrust fault (Fig. 2). This event may have occurred when the Sheep Mountain fault was locked and unable to continue propagating. Moreover, this younger fault would uplift the anticline. In the backlimb, we observed a second late fracture set, Set IV, which is composed of vertical joints striking 110° (Figs. 14 and 19). They are interpreted as late due to their vertical dip that is oblique to bedding. These joints may be related to the uplift. We suggest that this joint set orientation was influenced by the presence of the earlier Set I fractures, because they strike oblique to the fold axis and parallel to the Set I fractures. Such influence by pre-existing fractures has been suggested in recent studies (e.g. Guiton et al., 2003a,b; Bergbauer and Pollard, 2004).

6. Conclusions

Interpretations of the field data collected at Sheep Mountain, including fracture orientation, chronology, and mode of formation (opening vs. shearing), lead to the following conclusions regarding the structural evolution of the anticline. (i) A fracture set (Set I, 110°) was present before the onset of the Laramide compression. (ii) An early joint set (Set II, 045°) initiated during the beginning of the Laramide compression; however, the spatial distribution of this set was influenced by the onset of thrust faulting and/or folding. (iii) Set III joints (135°) localized in the hinge during layer bending related to fold evolution. Such joints also formed in the backlimb where sufficient bending occurred. (iv) Set I fractures were reactivated as reverse faults in the forelimb during late fold evolution. (v) Vertical joints (Set IV, 110°) oblique to the fold

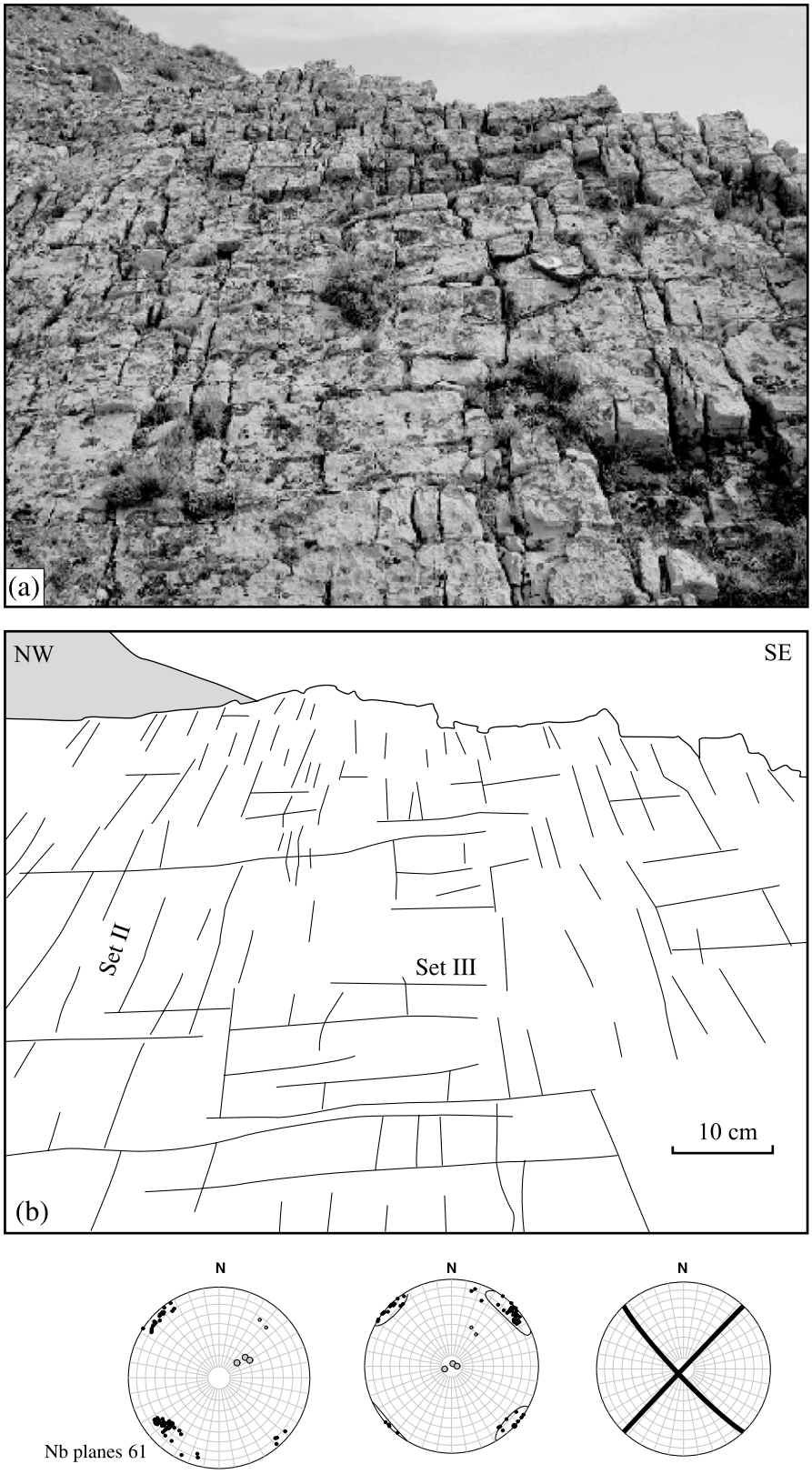

Fig. 18. Fracture pattern in the backlimb of the fold nose. (a) Field photograph showing the fracture pattern in the Phosphoria Fm. at site 2. (b) Line drawing of the outcrop in (a) showing that abutting relations are ambiguous among Sets II (045°) and III (135°). Polar stereonets left to right are present day fracture poles, pre-folding fracture poles, and great circles for mean orientations of each set. Poles to bedding are heavy circles.

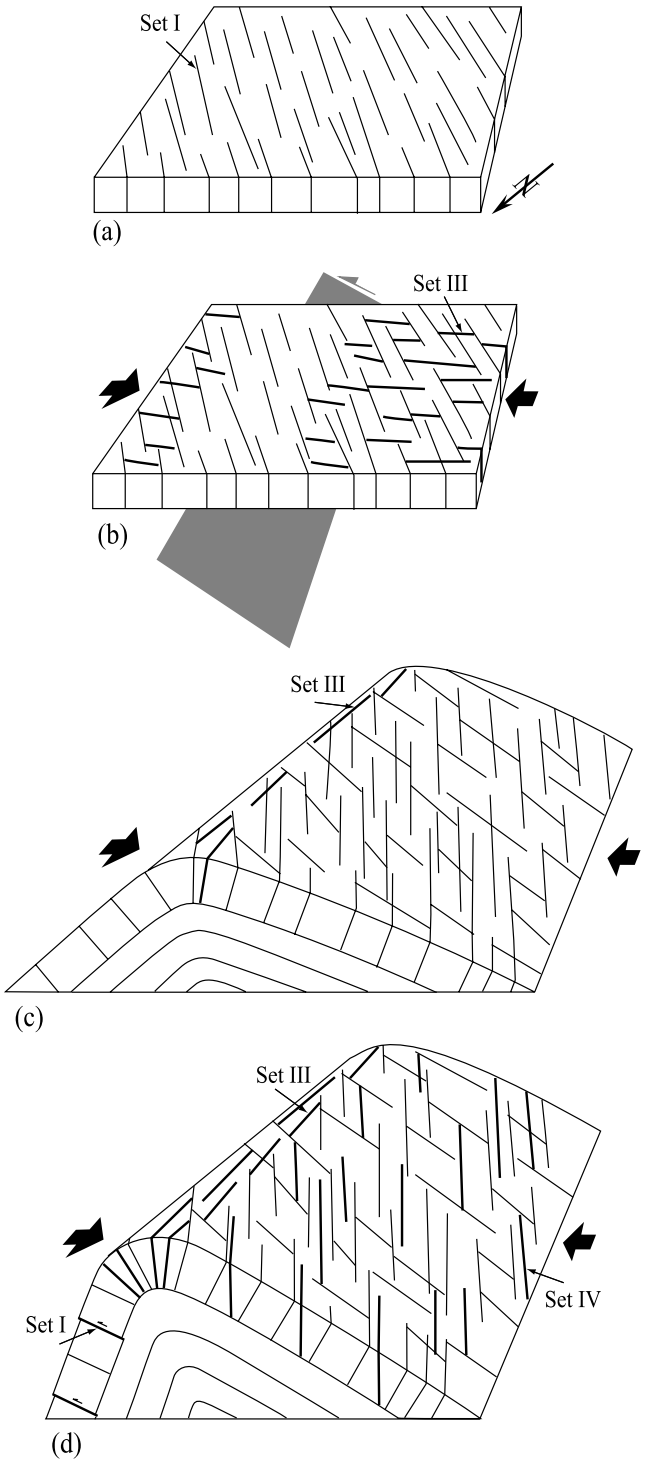

Fig. 19. Schematic representation of the fracturing history at Sheep Mountain anticline. (a) Set I (110°) fractures form in horizontal beds prior to the Laramide compression. (b) Set II (045°) joints as early compression-parallel fractures with underlying fault shown in gray. (c) Set III (135°) joints develop in the hinge during folding. (d) Vertical Set IV (110°) joints initiate parallel to Set I fractures in the backlimb, and Set I fractures are reactivated in forelimb as reverse faults during a late stage folding.

axis initiated in the backlimb, also during a late stage of folding. Their strike direction was controlled by the pre-existing fractures of Set I. The fracture data also constrain the folding kinematics. They suggest a fixed-hinge behavior of folding with little lateral propagation of the underlying thrust fault and the anticline. The data indicate that brittle deformation was concentrated in the fold hinge, but did occur in the limbs where curvature was significant, and during late stages of fold growth by fracture in-filling and reactivation.

Acknowledgements

This paper benefited from discussions with M. Cooke, J.M. Daniel, M. Guiton, and Y. Leroy. We thank E. Erslev and H. Stanton for providing a preprint of their paper, and I. Mynatt and Y. Fujii for assistance in the collection of fracture data in the field. J.M. Daniel and M. Guiton (Institut Français du Pétrole) are thanked for their help and for providing the software used to calculate mean fracture orientations and plot the data. The manuscript greatly benefited from the reviews of W. Dunne, C. Zahm, and C. Kluth. This work was supported by the National Science Foundation Tectonics Program Grant No. EAR-012935 and the Collaboration in Mathematical Geosciences Program Grant No. EAR-04177521, the Stanford Rock Fracture Project, and the Institut Français du Pétrole.

References

Allison, M.L., 1983. Deformation styles along the Tensleep fault, Bighorn Basin, Wyoming. Wyoming Geological Association Guidebook, 34th Annual Field Conference.

Allmendinger, R.W., 1982. Analysis of microstructures in the Meade plate of the Idaho–Wyoming foreland thrust belt (U.S.A.). Tectonophysics 85, 221–251.

Allmendinger, R.W., 1998. Inverse and forward numerical modeling of trishear fault-propagation folds. Tectonics 17, 640–656.

Antonellini, M.A., Aydin, A., Pollard, D.D., 1994. Microstructure of deformation bands in porous sandstones at Arches National Park, Utah. Journal of Structural Geology 16, 941–959.

Armstrong, P.A., Bartley, J.M., 1993. Displacement and deformation associated with a lateral thrust termination, southern Golden Gate Range, southern Nevada, U.S.A. Journal of Structural Geology 15, 721–735.

Aydin, A., 1978. Small faults formed as deformation bands in sandstone. Pure and Applied Geophysics 116, 913–930.

Bellahsen, N., Fiore, P., Pollard, D.D., 2006. Growth of basement fault-cored anticlines: the example of Sheep Mountain Anticline, Wyoming, Geophysical Research Letters 33, L02301, doi: 10.1029/2005GL024189.

Bergbauer, S., Pollard, D.D., 2004. A new conceptual fold–fracture model including prefolding joints, based on field data from the Emigrant Gap anticline, Wyoming. Geological Society of America Bulletin 116, 294–307.

Bernal, A., Hardy, S., 2002. Syn-tectonic sedimentation associated with three-dimensional fault-bend fold structures; a numerical approach. Journal of Structural Geology 24, 609–635.

Beutner, E.C., Diegel, F.A., 1985. Determination of fold kinematics from syntectonic fibers in pressure shadows, Marinsburg Slate, New Jersey. American Journal of Science 285, 16–50.

Bird, P., 1998. Kinematic history of the Laramide orogeny in latitudes 35°–49°N, western United States. Tectonics 17, 780–801.

Bird, P., 2002. Stress direction history of the Western United States and Mexico since 85 Ma. Tectonics 21, 1014. doi:10.1019/2001TC001319.

Bourne, S.J., Willemse, E.J.M., 2001. Elastic stress control on the pattern of tensile fracturing around a small fault network at Nash Point, UK. Journal of Structural Geology 23, 1753–1770.

Bump, A.P., 2003. Reactivation, trishear modeling, and folded basement in Laramide uplifts; implications for the origins of intra-continental faults. GSA Today 13, 4–10.

Chester, J., Chester, F., 1990. Fault-propagation folds above thrusts with constant dip. Journal of Structural Geology 12, 903–910.

Cooper, S.P., Goodwin, L.B., Lorenz, J.C., Teufel, L.W., Hart, B.S., 1998. Geometric and genetic relationships between fractures, normal faults, and a doubly plunging anticline; Teapot Dome, Wyoming. Geological Society of America, Abstracts with Programs 30, 62.

Couples, G., 1977. Stress and shear fracture (fault) patterns resulting from a suite of complicated boundary conditions with applications to the Wind River Mountains. Pure and Applied Geophysics 115, 113–133.

Cowie, P.A., Scholz, C.H., 1992. Physical explanation for the displacement–length relationship of faults using a post-yield fracture mechanics model. Journal of Structural Geology 14, 1113–1148.

Cristallini, E.O., Allmendinger, R.W., 2001. Pseudo 3-D modelling of trishear fault-propagation folding. Journal of Structural Geology 23, 1883–1899.

Cristallini, E.O., Allmendinger, R.W., 2002. Backlimb trishear; a kinematic model for curved folds developed over angular fault bends. Journal of Structural Geology 24, 289–295.

Dawers, N.H., Anders, M.H., Scholz, C.H., 1993. Growth of normal faults:displacement–length scaling. Geology 21, 1107–1110.

Dickinson, W.R., Snyder, W.S., 1978. Plate tectonics of the Laramide orogeny. Geological Society of America Memoir 151, 355–366.

Dunne, W.M., 1986. Mesostructural development in detached folds: an example from West Virginia. Journal of Geology 94, 473–488.

Engebretson, D.C., Cox, A., Gordon, R.G., 1985. Relative motion between oceanic and continental plates in the Pacific basin. Geological Society of America Special Paper 206, 59pp.

Engelder, T., Geiser, P., 1980. On the use of regional joint sets as trajectories of paleostress fields during the development of the Appalachian Plateau, New York. Journal of Geophysical Research 85, 6,319–6,341.

Engelder, T., Gross, M.R., Pinkerton, P., 1997. An analysis of joint development in thick sandstone beds of the Elk Basin Anticline, Montana-Wyoming. Rocky Mountain Association of Geologists 1997 Guidebook, Denver, Colorado, pp. 1–18.

Erslev, E.A., 1991. Trishear fault-propagation folding. Geology 19, 617–620.

Erslev, E.A., 1993. Thrusts, back-thrusts, and detachments of Rocky Mountain foreland arches. In: Schmidt, C.J., Chase, R.B., Erslev, E.A. (Eds.), Laramide Basement Deformation in the Rocky Mountain Foreland of the Western United States: Boulder, Colorado. Geological Society of America Special Paper 280, pp. 339–358.

Fischer, M.P., Christensen, R.D., 2004. Insights into the growth of basement uplifts deduced from a study of fracture systems in the San Rafael monocline, east central Utah. Tectonics 23, 1018. doi:10.1029/2002TC001470.

Fischer, M.P., Wilkerson, M.S., 2000. Predicting the orientation of joints from fold shape: results of pseudo-three-dimensional modeling and curvature analysis. Geology 28, 15–18.

Fischer, M., Woodward, N., Mitchell, M., 1992. The kinematics of break-thrust folds. Journal of Structural Geology 14, 451–460.

Fisher, D., Anastasio, D., 1994. Kinematic analysis of a large-scale leading-edge fold, Lost River range, Idaho. Journal of Structural Geology 16, 337–354.

Forster, A., Irmen, A.P., Vondra, C., 1996. Structural interpretation of Sheep Mountain Anticline, Bighorn Basin, Wyoming. Wyoming Geological Association Guidebook 47, 239–251.

Friedman, M., 1969. Structural analysis of fractures in cores from the Saticoy Field, Ventura Co., California. AAPG Bulletin 53, 367–389.

Frizon de Lamotte, D., Mercier, E., Dupre de la Tour, A., Averbuch, O., 1997. Cinématique du Plissement et Déformation Interne des Roches; l'exemple du pli de Lagrasse (Aude, France). Comptes Rendus de l'Académie des Sciences 324, 591–598.

Garfield, T.R., Hurley, N.F., Budd, D.A., 1992. Little Sand Draw File, Big Horn Basin, Wyoming: a hybrid dual-porosity and single-porosity reservoir in the Phosphoria Formation. AAPG Bulletin 76, 371–391.

Grelaud, S., Buil, D., Hardy, S., Frizon de Lamotte, D., 2000. Trishear kinematic model of fault-propagation folding and sequential development of minor structures: the Oupia anticline (NE Pyrenees, France) case study. Bulletin de la Société Géologique de France 171, 441–449.

Guiton, M., Leroy, Y., Sassi, W., 2003a. Activation of diffuse discontinuities and folding of the sedimentary layers. Journal of Geophysical Research 108, 2183. doi:10.1029/2002JB001770.

Guiton, M., Sassi, W., Leroy, Y., Gauthier, B., 2003b. Mechanical constraints on the chronology of fracture activation in the folded Devonian sandstone of the western Moroccan Anti-Atlas. Journal of Structural Geology 25, 1317–1330.

Hafner, W., 1951. Stress distribution and faulting. Bulletin of the Geological Society of America 62, 373–398.

Hancock, P.L., 1985. Brittle microtectonics; principles and practice. Journal of Structural Geology 7, 437–457.

Hardy, S., Ford, M., 1997. Numerical modeling of trishear fault propagation folding. Tectonics 16, 841–854.

Harris, J.F., Taylor, G.L., Walper, J.L., 1960. Relation of deformational fractures in sedimentary rocks to regional and local structures. AAPG Bulletin 44, 1853–1873.

Haws, G.W., Hurley, N.F., 1992. Applications of pressure-interference data in reservoir characterization studies, Big Horn basin, Wyoming. SPE 24668, presented at the 1992 Annual Conference and Exhibition, Washington D.C., October, pp. 53–62.

Hennier, J., 1984. Anticline, Bighorn Basin, Wyoming. Unpublished MS thesis, Texas A&M University, 118pp.

Hennier, J., Spang, J., 1983. Mechanisms for deformation of sedimentary strata at Sheep Mountain anticline, Big Horn Basin, Wyoming. Wyoming Geological Association Guidebook, 34th Annual Field Conference, pp. 97–111.

Hennings, P.H., Olson, J.E., Thompson, L.B., 2000. Combining outcrop data and three-dimensional structural models to characterize fractured reservoirs; an example from Wyoming. AAPG Bulletin 84, 830–849.

Homberg, C., Hu, J.C., Angelier, J., Bergerat, F., Lacombe, O., 1997. Characterization of stress perturbations near major fault zones: insights from 2-D distinct-element numerical modeling and field studies (Jura mountains). Journal of Structural Geology 19, 703–718.

Johnson, G.D., Garside, L.J., Warner, A.J., 1965. A study of the structure and associated features of Sheep Mountain Anticline, Big Horn County, Wyoming. Iowa Academy of Science 72, 332–342.

Johnson, K.M., Johnson, A.M., 2002. Mechanical analysis of the geometry of forced-folds. Journal of Structural Geology 24, 401–410.

Jamison, W.R., 1987. Geometric analysis of fold development in overthrust terranes. Journal of Structural Geology 9, 207–220.

Julian, F.E., Wiltschko, D.V., 1983. Deformation mechanism in a terminating thrust anticline. Geological Society of America, Program with Abstract 15, 606.

Kattenhorn, S.A., Aydin, A., Pollard, D.D., 2000. Joints at high angles to normal fault strike; an explanation using 3-D numerical models of fault-perturbed stress fields. Journal of Structural Geology 22, 1–23.

Kittler, J., 1976. A locally sensitive method for cluster analysis. Pattern Recognition 8, 23–33.

Ladd, R.E., 1979. The geology of Sheep Canyon Quadrangle: Wyoming. PhD dissertation. Ames, Iowa State University, 124pp.

Lajtai, E.Z., 1969. Mechanics of second order faults and tension gashes. Geological Society of America Bulletin 80, 2253–2272.

Maerten, L., Gillespie, P., Pollard, D.D., 2002. Effects of local stress perturbation on secondary fault development. Journal of Structural Geology 24, 145–153.

Mallet, J.L., 2002. Geomodeling. Oxford University Press, New York. 599pp.

Marcotte, D., Henry, E., 2002. Automatic joint set clustering using a mixture of bivariate normal distributions. International Journal of Rock Mechanics & Mining Sciences 39, 323–334.

Martel, S.J., Boger, W.A., 1998. Geometry and mechanics of secondary fracturing around small three-dimensional seismic data: evidence for dip linkage during fault growth. Journal of Geophysical Research 103, 21299–21308.

McConnell, D.A., 1994. Fixed-hinge, basement-involved fault-propagation folds, Wyoming. Geological Society of America Bulletin 106, 1583–1593.

Mitra, S., 1990. Fault-propagation folds: geometry, kinematic evolution, and hydrocarbon traps. AAPG Bulletin 74, 921–945.

Nickelsen, R.P., 1979. Sequence of structural stages of the Alleghany Orogeny at the Bear Valley strip mine, Shamokin, Pennsylvania. American Journal of Science 279, 225–271.

Nino, F., Philip, H., Chery, J., 1998. The role of bed-parallel slip in the formation of blind thrust faults. Journal of Structural Geology 20, 503–516.

Peacock, D.C.P., Sanderson, D.J., 1991. Displacements, segment linkage and relay ramps in normal fault zones. Journal of Structural Geology 13, 721–733.

Pollard, D.D., Aydin, A., 1988. Progress in understanding jointing over the past century. Geological Society of America Bulletin 100, 1181–1204.

Pollard, D.D., Segall, P., 1987. Theoretical displacements and stresses near fractures in rocks: with applications to faults, joints, veins, dikes, and solution surfaces. In: Atkinson, B.K. (Ed.), Fracture Mechanics of Rock. Academic Press, London, pp. 277–349.

Price, N., 1966. Fault and Joint Development in Brittle and Semi-brittle Rock. Pergamon Press, Oxford. 176pp.

Price, N.J., Cosgrove, J.W., 1990. Analysis of Geological Structures. Cambridge University Press, Cambridge. 502pp.

Rawnsley, K.D., Rives, T., Petit, J.-P., Hencher, S.R., Lumsden, A.C., 1992. Joint development in perturbed stress fields near faults. Journal of Structural Geology 14, 939–951.

Reches, Z., Lockner, D.A., 1994. Nucleation and growth of faults in brittle rocks. Journal of Geophysical Research 99, 18159–18173.

Rioux, R.L., 1958. Geology of the Spence-Kane area, Bighorn County, Wyoming. Unpublished Ph.D. thesis, University of Illinois, 182pp.

Rioux, R.L., 1994. Geologic map of the Sheep Mountain–Little Sheep Mountain area, Big Horn County, Wyoming. Scale 1:31,680. USGS open-file report 94-191.

Savage, H.M., Cooke, M.L., 2004. The effect of non-parallel thrust fault interaction on fold pattern. Journal of Structural Geology 26, 905–917.

Segall, P., Pollard, D., 1980. Mechanics of discontinuous faults. Journal of Geophysical Research 88, 555–568.

Silliphant, L.J., Engelder, T., Gross, M.R., 2002. The state of stress in the limb of the Split Mountain anticline, Utah: constraints placed by transected joints. Journal of Structural Geology 24, 155–172.

Simmons, S.P., Scholle, P.A., 1990. Late Paleozoic uplift and sedimentation, Northeast Bighorn Basin, Wyoming. Wyoming Geological Association, Guidebook 41, 39–55.

Shamir, G., Eyal, Y., 1995. Elastic modeling of fault-driven monoclinal fold patterns. Tectonophysics 245, 13–24.

Spang, J.H., McConnell, D.A., 1997. Effect of initial fault geometry on the development of fixed-hinge, fault-propagation folds. Journal of Structural Geology 19, 1537–1541.

Stanton, H.I., Erslev, E.A., 2004. Sheep Mountain Anticline: backlimb tightening and sequential deformation in the Bighorn Basin, Wyoming. Wyoming Geological Association Guidebook 53, 75–87.

Stearns, D.W., 1968. Certain aspects of fractures in naturally deformed rocks. Rock Mechanics Seminar. R.E. Riecker, Bedford, Terrestrial Sciences Laboratory, pp. 97–118.

Stearns, D.W., Friedman, M., 1972. Reservoirs in fractured rocks. American Association of Petroleum Geologists Memoir 16, 82–100.

Stone, D.S., 1993. Basement-involved thrust generated folds as seismically imaged in sub-surface of the central Rocky Mountain foreland. In: Schmidt, C.J., Chase, R.B., Erslev, E.A. (Eds.), Laramide Basement Deformation in the Rocky Mountain Foreland of the Western United States Geological Society of America Special Paper 280, pp. 271–318.

Stone, D.S., 2004. Rio thrusting, multi-stage migration, and formation of vertically segregated Paleozoic oil pools at Torchlight Field on the Greybull Platform (Eastern Bighorn basin): implications for exploration. The Mountain Geologist 41, 119–138.

Storti, F., Salvini, F., McClay, K., 1997. Fault-related folding in sandbox analogue models of thrust wedges. Journal of Structural Geology 19, 583–602.

Suppe, J., 1983. Geometry and kinematics of fault-bend folding. American Journal of Science 283, 684–721.

Suppe, J., 1985. Principles of Structural Geology. Prentice-Hall, Englewood Cliffs, New Jersey. 537pp.

Suppe, J., Medwedeff, D.A., 1990. Geometry and kinematics of fault-propagation folding. Eclogae Geologicae Helvetica 83, 409–454.

Thomas, L.E., 1965. Sedimentation and structural development of the Bighorn Basin. American Association of Petroleum Geologists Bulletin 49, 1867–1877.

Walsh, J.J., Nicol, A., Childs, C., 2002. An alternative model for the growth of faults. Journal of Structural Geology 24, 1669–1675.

Wicks, J.L., Dean, S.L., Kulander, B.R., 2000. Regional tectonics and fracture patterns in the Fall River Formation (Lower Cretaceous) around the Black Hills foreland uplifts, western South Dakota and northeastern Wyoming. In: Cosgrove, J.W., Ameen, M.S. (Eds.), Forced Folds and Fractures Geological Society of London Special Publication 169, pp. 145–165.

Wollmer, F.W., 1995. C Program for automatic contouring of spherical orientation data using a modified Kamb method. Computers & Geosciences 21, 31–49.

Ye, H., Royden, L., Burchfiel, C., Schuepbach, M., 1996. Late Paleozoic deformation of interior North America: the Greater Ancestral Rocky Mountains. American Association of Petroleum Geologists Bulletin 80, 1397–1432.

Zhang, Y., Mancktelow, N.S., Hobbs, B.E., Ord, A., Mühlhaus, H.B., 2000. Numerical modelling of single-layer folding: clarification of an issue regarding the effect of computer codes and the influence of initial irregularities. Journal of Structural Geology 22, 1511–1522.